of TR-BBB13 cells relative to the quantity of β-actin. The control lacking the RT enzyme was assayed in parallel to monitor any possible genomic contamination. The PCR was performed through 40 cycles of 95°C for 30 s, 60°C for 1 min, and 72°C for 1 min after preincubation at 95°C for 10 min using specific primers. The sequences of the primers were as follows: sense primer (S1) 5′-CAATGGGATCATGAAACCTG-3′ and antisense primer (AS1) 5′-GAGGCTGATGAATGGAGAA-3′ for ABCG2 (GenBank accession number NM011920); sense primer 5′-TTTGAGACCTTCAA CACCCC-3′ and antisense primer 5′-ATAGCTCTTCTCCAGG GAGG-3′ for β-actin (GenBank accession number NM031144).

Isolation of rat homologue of ABCG2 (rABCG2) cDNA

Rat brain capillary fraction was collected from brain homogenates as described previously (Hosoya *et al.* 2000b). Briefly, cerebrum excised from rats was dissected into 2-mm pieces, and homogenized using a Potter-Elvehjem homogenizer in PBS. Homogenate was added to the same volume of 32% dextran solution, and then centrifuged (4500 × *g*, 10 min, 4°C). The resulting pellets were washed in PBS to obtain the enriched capillary fraction. Total RNA was extracted from rat brain capillary fraction with TRIZOL reagent according to the manufacturer's protocol. To prepare 5′- or 3′-cDNA fragments, the total RNA was reverse-transcribed by PowerScript™ RT enzyme (BD Biosciences) in the presence of modified oligo (dT) primers, which contain sequences for annealing with Universal Primer Mix (UPM) (BD Biosciences). After generation of the 5′- and 3′-cDNA fragments, 5′- or 3′-RACE PCR was performed using two sets of primers (UPM and 5′RACE 1, or UPM and 3′RACE1, respectively) and Advantage 2 Polymerase (BD Biosciences). The sequences of the primers were as follows: 5′RACE 1 primer 5′-CCCCGTGGGTCTTTCCTTGCTGCTAGG-3′, 3′RACE1 primer 5′-CTGGCCATAGCCGCAGGCCAAAGCG-3′.

To obtain three overlapping PCR products, PCR was performed using three sets of primers (S1 and AS1, S2 and AS2, and S3 and AS3) with Ex Taq (Takara, Shiga, Japan). The sequences of S1 and AS1 primers are given above. The sequences of the other primers were as follows: S2 primer 5′-GGACTCAAGCACAGCAAATGC-3′, AS2 primer 5′-CTCCACAGCTGACACACTG-3′, S3 primer 5′-CCTGACTACCAACCAGTG-3′ and AS3 primer 5′-GCTGTGAAGCCATATCGAGG-3′. All PCR procedures were performed at least twice, and the PCR products were subcloned into a plasmid vector using pGEM-T Easy Vector and amplified in *Escherichia coli*. Several independent clones obtained from each PCR procedure were sequenced from both directions using a DNA sequencer (CEQ2000XL DNA Analysis System; Beckman Coulter, Fullerton, CA, USA).

Construction of plasmid vector and transfectant

rABCG2 cDNA was generated by RT-PCR from total RNA of rat brain capillary fraction with the following primers: sense primer with a BamHI site (underlined), 5′-GGATCCGATGTCTTCTAGT-AATGAC-3′, antisense primer with an XhoI site (underlined), 5′-CTCGAGCAATAGTCCTTTCAAGGG-3′. The PCR product was subcloned into a plasmid vector using the pGEM-T Easy vector for sequencing. The cDNA segment 100% identical with the full-length of rABCG2 was cut from pGEM-T Easy with BamHI and XhoI (Takara), and ligated into pCMV-Tag3A (Stratagene, La Jolla, CA, USA), which contains the c-myc epitope (EQKLISEEDL) from the human c-myc gene in the upstream of the multiple cloning site (pCMV-Tag3A/rABCG2). To obtain rABCG2-overexpressing cells, pCMV-Tag3A/rABCG2 was transfected into HEK293 cells using Lipofectamine plus (Life Technologies) according to the manufacturer's procedure. G418 (800 μg/mL)-resistant cells were picked up, and myc-tagged rABCG2-expressing cells (HEK293/rABCG2myc) were selected by western blot analysis of ABCG2.

Antibody preparation

Polyclonal antibodies to ABCG2 were raised against amino acid residues 1–34 (G2-Ab1) and 305–343 (G2-Ab2) of mouse ABCG2 (GenBank accession number AF140218). The polypeptides were expressed as glutathione *S*-transferase (GST) fusion proteins using pGEX4T-2 plasmid vector (Amersham Biosciences, Uppsala, Sweden). The fusion protein was purified with glutathione-Sepharose 4B (Amesham Biosciences), emulsified with Freund's complete adjuvant (Difco, Detroit, MI, USA), and injected subcutaneously into female Hartley guinea pigs at intervals of two weeks. Two weeks after the sixth injection, affinity-purified antibodies were prepared, first using protein G-Sepharose (Amersham Biosciences) and then using antigen peptides coupled to cyanogen bromide-activated Sepharose 4B (Amersham Biosciences). For the preparation of affinity media, polypeptides devoid of GST were obtained by elution of the cleaved polypeptide after in-column thrombin digestion of fusion proteins bound to glutathione-Sepharose.

Western blot analysis

Rat tissues were obtained after perfusion in the same way as for the quantitative real-time PCR analysis. Rat tissues, HEK293 cells, HEK293/rABCG2myc cells, or TR-BBB13 cells were homogenized in buffer containing 10 mM Tris-HCl (pH 7.4), 10 mM NaCl, 1.5 mM $MgCl_2$, 1 mM phenylmethylsulfonyl fluoride (PMSF), and a protease-inhibitor cocktail (Sigma Chemical Co., St. Louis, MO, USA). The homogenized samples were centrifuged at 10 000 × *g* for 10 min and the supernatants were collected. These supernatants were centrifuged at 100 000 × *g* for 30 min, and a crude membrane fraction was obtained from the pellets. The pellets were suspended in buffer containing 10 mM Tris-HCl (pH 7.4), 1 mM EDTA, 150 mM NaCl, 4% CHAPS, 1 mM PMSF, and a protease-inhibitor cocktail. The protein concentration of the lysates was measured by the Bradford method using Bio-Rad Protein Assay reagent (Bio-Rad, Hercules, CA, USA). Deglycosylation was carried out by incubating the crude membrane protein fraction with *N*-glycosidase F (Boehringer Mannheim) for 30 min at 37°C. Protein samples (tissues, 20 μg; TR-BBB13 cells, 80 μg per lane) were resolved by 7.5% SDS–polyacrylamide gel (Bio-Rad) electrophoresis and subsequently electrotransferred to nitrocellulose membranes. Membranes were treated with blocking buffer (4% skimmed milk in 25 mM Tris-HCl (pH 8.0), 125 mM NaCl, 0.1% Tween 20) for 2 h at room temperature and incubated with anti-ABCG2 antibodies (G2-Ab1, 1 μg/mL for HEK293/rABCG2myc cells, rat tissues and TR-BBB13 cells; G2-Ab2, 0.5 μg/mL for HEK293/rABCG2myc cells) or anti-c-myc antibody (0.1 μg/mL; Bethyl Laboratories, Montgomery, TX, USA) as the primary antibody at 4°C for 16 h after blocking. The membranes were washed three times with blocking buffer and incubated with horseradish peroxidase-conju-

gated second antibody. The bands were visualized with an enhanced chemiluminescence kit (SuperSignal; Pierce, Rockford, IL, USA).

Immunohistochemical analysis in HEK293/rABCG2myc cells and rat brain

HEK293 cells or HEK293/rABCG2myc cells were seeded at a density of 5×10^4 cells on chamber slides (4.0 cm^2; Asahi Techno Glass Corp., Tokyo, Japan), and cultured overnight. The following procedures were carried out at room temperature. Cells were washed with PBS and fixed with 4% paraformaldehyde in PBS for 20 min. Cells were incubated with 0.1% Triton X-100 in PBS for 30 min and then incubated with 10% goat serum for 30 min. After further washing with PBS, the cells were incubated with anti-c-myc antibody (1 μg/mL; Santa Cruz Biotechnology, Santa Cruz, CA, USA) as a primary antibody in the presence of 0.1% bovine serum albumin in PBS for 1 h. Cells were then washed with PBS and incubated for 1 h with fluorescein isothiocyanate (FITC)-conjugated second antibody for 1 h. Cells were washed with PBS and immunofluorescence was viewed using a confocal laser scanning microscope (TCS SP, Leica Microsystems, Wetzlar, Germany).

Under deep pentobarbital anesthesia (100 mg/kg of body weight), brains of adult Wistar rats were perfused transcardially with 4% paraformaldehyde in 0.1 M sodium phosphate buffer (PB), pH 7.4, embedded in paraffin wax after dehydration using graded alcohols, and processed for the preparation of paraffin sections (5 μm) with a sliding microtome (SM2000R; Leica Microsystems). Prior to immunohistochemical investigation, paraffin sections were digested with pepsin (1 mg/mL in 0.2 M HCl, Dako, Carpinteria, CA, USA) for 5 min at 37°C to retrieve antigens. For immunofluorescence, sections were incubated at room temperature with 10% normal goat serum for 30 min, guinea pig anti-ABCG2 antibody (G2-Ab2) 2 μg/mL singly or in combination with rabbit glucose transporter 1 (GLUT1) antibody (1 : 5000; Chemicon, Temecula, CA, USA) overnight, FITC- or rhodamine-conjugated secondary antibody for 2 h. Some sections were counterstained with 3 μg/mL propidium iodide for 5 min. Photographs were taken with a confocal laser scanning microscope (TCS SP, Leica Microsystems).

Transport assay

For transport studies, HEK293 cells or HEK293/rABCG2myc cells were incubated for 30 min at 37°C in a medium, with or without 10 μM Ko143, a specific ABCG2 inhibitor. After the 30-min preincubation period, the cells were washed with ice-cold medium, resuspended in a medium containing 20 μM mitoxantrone, with or without 10 μM Ko143, and incubated for a further 1 h at 37°C. The cells were then washed with ice-cold PBS and placed on ice until required for measurement. For efflux studies, the cells were incubated for 60 min at 37°C with BODIPY-prazosin (250 nM) (Molecular Probes, Eugene, OR, USA) and then allowed to efflux for 30 min in a medium, with or without 10 μM Ko143. The cells were then washed with ice-cold PBS and placed on ice until required for measurement. Relative cellular accumulation of BODIPY-prazosin and mitoxantrone was determined by flow cytometry with a 488 nm argon laser/530 nm bandpass filter and a 635 nm red diode laser/661 nm bandpass filter, respectively (FACs Calibur; BD Biosciences). At least 20 000 events were collected. Debris was eliminated by gating on forward versus side scatter. The mean channel number for each histogram was used as a measure of drug fluorescence for the calculation.

Effects of conditioned medium of TR-AST4 cells (AST-CM) and TR-PCT1 cells (PCT-CM) on the drug transport activity in TR-BBB13 cells

AST-CM and PCT-CM were obtained as described previously (Hori *et al.* 2004). TR-BBB13 cells were seeded at a density of 1×10^5 cells/well on rat-tail collagen I-coated 24-well plates (BD Biosciences) and cultured for 24 h at 33°C. TR-BBB13 cells were treated with AST-CM or PCT-CM for 24 h at 33°C. After removal of the culture medium, the cells were washed with extracellular fluid (ECF) buffer (122 mM NaCl, 25 mM $NaHCO_3$, 3 mM KCl, 1.4 mM $CaCl_2$, 2 mM $MgSO_4$, 0.4 mM K_2HPO_4, 10 mM D-glucose, 10 mM HEPES (pH 7.4), 290 ± 15 mOsm/kg). The transport study was performed at 37°C, the physiological temperature. The cells were pretreated at 37°C for 30 min in the presence or the absence of 0.5 μM Ko143, then uptake was initiated by adding ECF buffer containing 20 μM mitoxantrone or 250 nM BODIPY-prazosin, with or without Ko143, and incubation was continued for a further 1 h at 37°C. The efflux transport activity was terminated by removing the solution and immersing the cells in ice-cold ECF buffer. The cells were collected and placed on ice until required for measurement. Flow cytometry analysis was performed as described above.

Data analysis

Unless otherwise indicated, all data represent the mean ± SEM. An unpaired, two-tailed Student's *t*-test was used to determine the significance of differences between two groups means. One-way ANOVA followed by the modified Fisher's least-squares difference method was used to assess the statistical significance of differences among means of more than two groups.

Results

mRNA expression of ABCG2 in rat brain capillary fraction and tissues

Quantitative real-time PCR analysis was performed to determine the ABCG2 mRNA levels in rat brain capillary fraction, small intestine, kidney, heart and brain (Fig. 1a). High mRNA expression of ABCG2 was detected in rat brain capillary fraction. When each mRNA level was indicated as a relative ratio to that in rat small intestine, the ABCG2 mRNA levels in rat kidney, heart, brain and brain capillary fraction were 1.16 ± 0.17, 0.23 ± 0.02, 0.19 ± 0.03 and 6.59 ± 0.46, respectively. Moreover, the ABCG2 mRNA level in the rat brain capillary fraction was enriched by 34.7-fold compared with that in rat brain.

cDNA cloning of rat homologue of ABCG2 (rABCG2) from rat brain capillary fraction

rABCG2 cDNA was isolated from the rat brain capillary fraction. The cDNA sequence (GenBank accession number AB105817) has a single open reading frame (1974 bp),

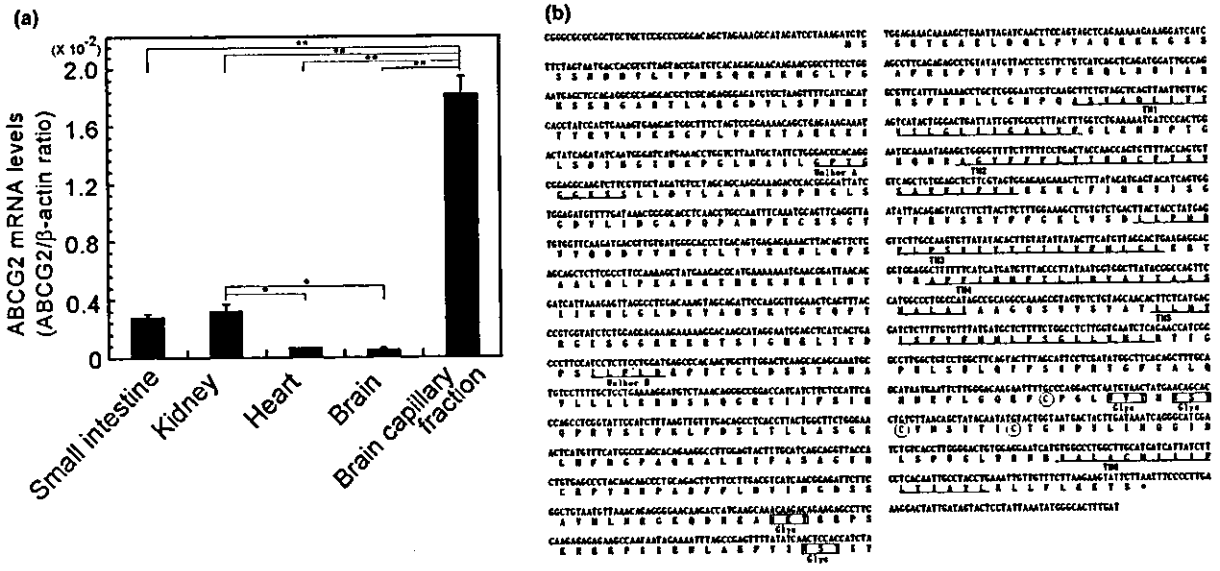

Fig. 1 rABCG2 cDNA cloning from rat brain capillary fraction. (a) The ABCG2 mRNA levels in rat brain capillary fraction and other tissues were determined by quantitative real-time PCR analysis. Each column represents the mean SEM ($n = 3$). $^{**}p < 0.01$, $^{*}p < 0.05$, significant difference. (b) Nucleotide sequence and deduced amino acid sequence of rABCG2 cDNA. The deduced amino acid sequence is shown below the nucleotide sequence. The Walker A and B motifs, and six putative transmembrane domains (TM1-6) are underlined. Open circles indicate potential sites for disulfide bonds. Glyc, potential N-glycosylation sites; GenBank accession number AB105817.

which corresponds to 657 amino acid residues (Fig. 1b). Its deduced amino acid sequence is 81.2, 93.0 and 80.7% identical with human, mouse and porcine ABCG2, respectively. Further amino acid analysis revealed that the ATP-binding domain is located at position 54–268. This domain includes the Walker A and B motifs at 79–86 (GPTGGGKS) and 205–209 (ILFLD), respectively. This N-terminal region includes six putative TM domains (TM1-6) (Fig. 1b). Four potential sites for N-linked glycosylation are shown in Fig. 1(b). Two N-linked glycosylation sites are located in the loop between TM5 and TM6 at amino acid positions 596–699 (NVT) and 600–602 (NST), and are probably extracellular. The other N-linked glycosylation sites are located at amino acid positions 316–319 (NKT) and 338–340 (NST), which is likely to be in the intracellular part of the protein. Three potential sites for disulfide bonds are located in the loop between TM5 and TM6 at amino acid positions 592 (C), 603 (C) and 610 (C). The sequence of the open reading frame of rABCG2 cDNA in TR-BBB13 cells showed 100% homology with that in rat brain capillary fraction.

Expression and plasma membrane localization of myc-tagged rABCG2 protein in HEK293 cells

The expression of myc-tagged rABCG2 was determined by western blot analysis using anti-c-myc and anti-ABCG2 antibodies (G2-Ab1 and G2-Ab2) (Fig. 2a,b). At the same time, the specificity of G2-Ab1 and G2-Ab2 against rABCG2 was evaluated. In the presence of a reducing agent (2-mercaptoethanol), a single band at ~85 kDa was detected in HEK293/rABCG2myc cells with anti-c-myc antibody, whereas no band was detected in parental HEK293 cells (Fig. 2a). The ~85-kDa protein was also detected with G2-Ab1 and G2-Ab2 (Fig. 2a). In the absence of the reducing agent, bands at ~85 kDa and ~170 kDa were detected in HEK293/rABCG2myc cells with anti-c-myc antibody, G2-Ab1 and G2-Ab2 (Fig. 2b).

Figure 2(c) shows the confocal microscopic images of HEK293/rABCG2myc cells stained with anti-c-myc antibody. Intense immunoactivities at the plasma membrane were detected in HEK293/rABCG2myc cells treated with anti-c-myc antibody, whereas no signals were seen in HEK293/rABCG2myc cells treated with normal mouse immunoglobulin and in the parental cells (HEK293 cells) treated with anti-c-myc antibody (data not shown).

Mitoxantrone and BODIPY-prazosin efflux mediated by rABCG2

The mitoxantrone level in HEK293/rABCG2myc cells was significantly reduced compared with that in HEK 293 cells (the parental cells) (Fig. 3a). Figure 3(a) also shows the effects of various concentrations of Ko143, a specific inhibitor of mouse and human ABCG2, on mitoxantrone accumulation in HEK293/rABCG2myc cells, as measured by

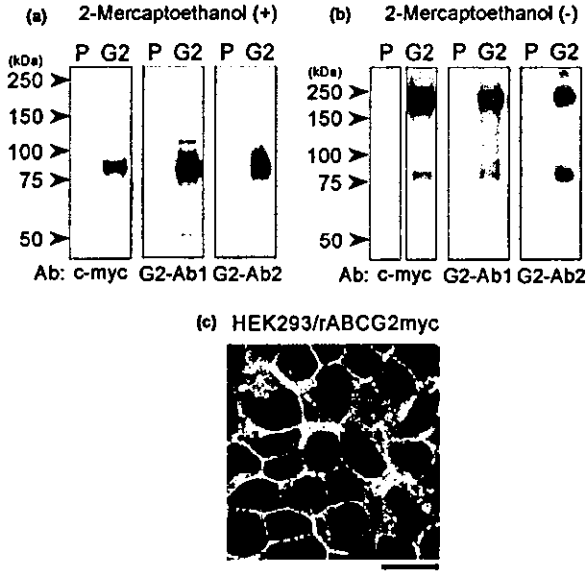

Fig. 2 Expression and localization of myc-tagged rABCG2 in transfected HEK293 cells. (a,b) Western blot analysis using anti-c-myc or anti-ABCG2 (G2-Ab1 and G2-Ab2) antibodies (Ab) against HEK293 cells (P) and HEK293/rABCG2myc cells (G2) in the presence (a) or absence (b) of 2-mercaptoethanol. (c) Immunostaining of myc-tagged rABCG2 in HEK293/rABCG2myc cells. Anti-c-myc antibody was used for immunostaining. Scale bar, 20 μm.

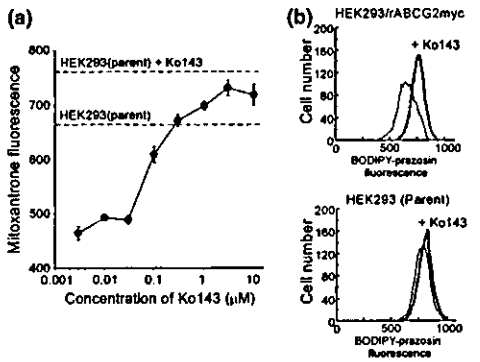

Fig. 3 Functional analysis of rABCG2 in rABCG2-overexpressing cells. (a) Concentration-dependent effect of Ko143 treatment on the intercellular accumulation of mitoxantrone in HEK293/rABCG2myc cells. Horizontal dashed lines show levels of mitoxantrone fluorescence in the parental HEK293 cells in the presence or absence of 10 μM Ko143. Mitoxantrone fluorescence in arbitrary units was determined by flow cytometry with a 635/661 nm filter. Each point represents the mean ± SEM ($n = 4$). (b) Effect of Ko143 (10 μM) on the BODIPY-prazosin (250 nM) efflux in parental HEK293 cells and HEK293/rABCG2myc cells. BODIPY-prazosin fluorescence is in arbitrary units, determined by flow cytometry with a 488/530 nm filter.

flow cytometry. In HEK293/rABCG2myc cells, mitoxantrone levels were elevated by Ko143 treatment in a concentration-dependent manner at concentrations over 0.01 μM, reaching a plateau at 3 μM. In contrast, Ko143 had only a small effect on mitoxantrone levels in the parental HEK293 cells. Based on the midpoint of the cellular accumulation curve in Fig. 3(a), the concentration of Ko143 was approximately 0.1 μM. This value was very close to that in cells overexpressing human ABCG2 (IGROV1/T8 cells) and mouse ABCG2 (MEF3.8/T6400 cells) (Allen *et al.* 2002), suggesting that the inhibitory effect of Ko143 on the ABCG2-mediated transport is essentially the same in rats, humans and mice.

The effect of Ko143 (10 μM) treatment on BODIPY-prazosin efflux is shown in the histograms of Fig. 3(b). In HEK293/rABCG2myc cells, BODIPY-prazosin efflux was inhibited by Ko143 treatment. In contrast, Ko143 had only a small effect on BODIPY-prazosin efflux in the parental HEK293 cells.

Expression and N-linked glycosylation of rABCG2 protein in rat brain capillary fraction and other rat tissues

As rABCG2 has potential N-linked glycosylation sites (Fig. 1b), western blot analysis of rABCG2 was performed with or without *N*-glycosidase F using a crude membrane fraction of rat brain capillary fraction and tissues (Fig. 4a). In the absence of *N*-glycosidase F, bands were detected at

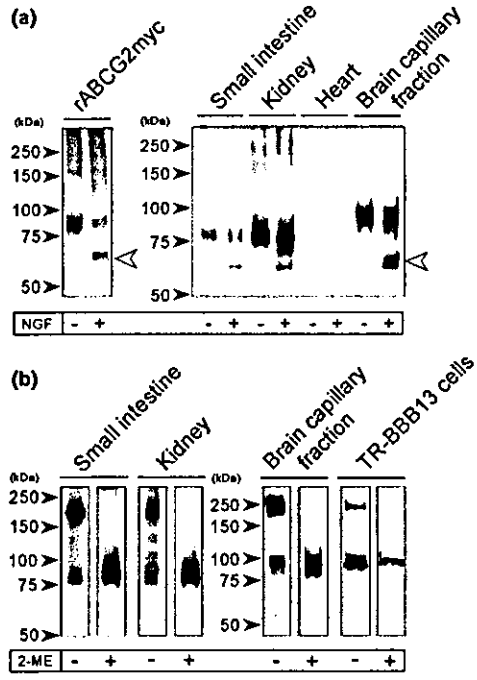

Fig. 4 Western blot analysis of rABCG2 in rat brain capillary fraction, TR-BBB13 cells and other tissues. (a) Protein samples were incubated in the presence (+) or absence (–) of *N*-glycosidase F (NGF). Open arrowheads indicate the expected size of rABCG2. rABCG2myc, HEK293/rABCG2myc cells. (b) Protein samples were incubated in the presence (+) or absence (–) of 2-mercaptoethanol (2-ME).

~85 kDa in rat small intestine and kidney, and at ~100 kDa in rat brain capillary fraction, while no bands were detected in rat heart. Following treatment with *N*-glycosidase F, part of the bands corresponding to rABCG2 shifted to 62 kDa in the apparent molecular mass of bands in rat small intestine, kidney and brain capillary fraction. The 62-kDa band was also detected in HEK293/rABCG2myc cells treated with *N*-glycosidase F.

Disulfide complex of rABCG2 protein in rat brain capillary fraction, TR-BBB13 cells and other rat tissues

Western blot analysis was performed on rat small intestine, kidney, brain capillary fraction and TR-BBB13 cells with or without 2-mercaptoethanol, a reducing agent, in order to clarify whether rABCG2 forms a complex via disulfide bonds (Fig. 4b). In rat small intestine and kidney, single bands at ~85 kDa were detected under reducing conditions. A high-molecular band at ~170 kDa, in addition to the band at ~85 kDa, was also detected under non-reducing conditions. In rat brain capillary fraction, high-molecular bands at ~200 kDa, and ~100 kDa, were detected under non-reducing conditions. In TR-BBB13 cells, two bands were detected at the same position as that of the disulfide-linked complex in rat brain capillary fraction.

Immunostaining of rABCG2 in the cerebral cortex of rat brain

The localization of rABCG2 was determined in the cerebral cortex of adult rats. rABCG2 immunoreactivities were strongly detected in brain capillaries, which are ramified in all cortical layers (Fig. 5a). Immunostaining was observed along the surface of capillaries (Fig. 5b), and was localized to the inner side of capillary endothelium nuclei (Fig. 5b,c, arrowheads). Double immunostaining with GLUT1 (Fig. 5e,f, red), which is known to be expressed in both the luminal and abluminal membrane of brain capillaries (Dobrogowska and Vorbrodt 1999), showed that rABCG2 (Fig. 5d,f, green) overlapped on the luminal membrane of capillaries (arrowheads), but was below the detection threshold on the abluminal membrane (arrows). Such characteristic immunostaining was not seen following the use of preimmune guinea pig immunoglobulin (data not shown). These features indicate that rABCG2 is preferentially expressed on the luminal membrane of rat brain capillaries.

Enhancement of rABCG2-mediated transport in TR-BBB13 cells following treatment with AST-CM

The mitoxantrone and BODIPY-prazosin levels in TR-BBB13 cells reached a steady state after 45 min (data not shown). Ko143 treatment increased the mitoxantrone and BODIPY-prazosin levels in TR-BBB13 cells at 60 min (Fig. 6a,b, control). As Ko143 is a selective inhibitor of ABCG2, as shown by the fact that 0.5 μM Ko143 had little effect on P-gp or MRP1-5 (Allen *et al.* 2002), the Ko143-dependent enhancement of drug transport activity should reflect the inhibition of ABCG2-mediated drug efflux.

The mitoxantrone and BODIPY-prazosin levels were reduced in TR-BBB13 cells at 60 min by treatment with one- to five-fold concentrated AST-CM (Fig. 6a,b). In contrast, PCT-CM did not affect the level of either drug (Fig. 6a,b). Ko143 treatment reversed the fall in the levels of both drugs (Fig. 6a,b, open columns). Moreover, the Ko143-sensitive transport activity of BODIPY-prazosin was significantly increased by treatment with one- to five-fold concentrated AST-CM compared with non-treated cells, and that of mitoxantrone also showed a tendency to increase (Fig. 6c).

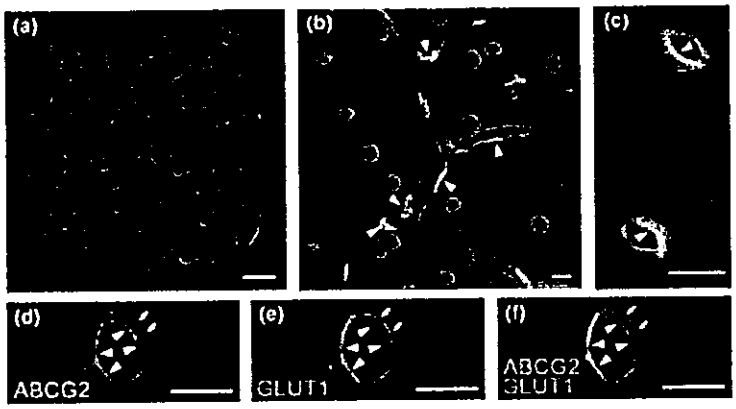

Fig. 5 Immunostaining of rABCG2 in the cerebral cortex of rat brain. (a–c) Low (a) and high (b,c) magnification views of rABCG2 immunostaining in the cerebral cortex. Nuclei were stained by propidium iodide (red; b, c). rABCG2 immunoreactivities (green) were detected in the inner side of capillary endothelium nuclei (arrowheads; b, c). (d–f) Double immunostaining of rABCG2 (green; d, f) and GLUT1 (red; e, f). rABCG2 immunoreactivities were detected on the luminal membrane of capillaries (arrowheads), but not on the abluminal membrane (arrows). Scale bars; (a) 100 μm, (b–f) 10 μm.

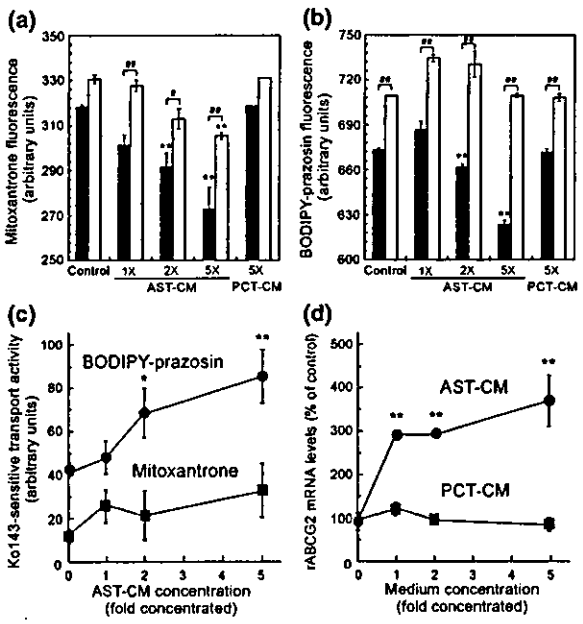

Fig. 6 Functional enhancement of rABCG2 in TR-BBB13 cells produced by treatment with conditioned medium of TR-AST4 cells. (a,b) Effects of one-, two- and five-fold concentrated AST-CM and fivefold concentrated PCT-CM treatment on mitoxantrone (a) and BODIPY-prazosin (b) fluorescence in TR-BBB13 cells in the absence (black columns) or presence (open columns) of 0.5 μM Ko143. Mitoxantrone and BODIPY-prazosin fluorescence in arbitrary units were determined by flow cytometry with a 635/661 nm filter and a 488/530 nm filter, respectively. Each column represents the mean ± SEM ($n = 3$). $^{**}p < 0.01$, significantly different from the respective control. $^{\#\#}p < 0.01$, $^{\#}p < 0.05$, significant difference. (c) The Ko143-sensitive mitoxantrone (■) and BODIPY-prazosin (●) levels in TR-BBB13 cells following treatment with one-, two- and five-fold concentrated AST-CM. The mitoxantrone and BODIPY-prazosin levels are in arbitrary units. Each point represents the mean ± SEM ($n = 3$). $^{**}p < 0.01$, $^{*}p < 0.05$, significantly different from the control. (d) Effects of AST-CM (●) and PCT-CM (■) on the rABCG2 mRNA levels in TR-BBB13 cells for 24 h. The rABCG2 mRNA levels were determined by quantitative real-time PCR analysis. Each point represents the mean ± SEM ($n = 3$). $^{**}p < 0.01$, significantly different from the control.

Induction of rABCG2 mRNA in TR-BBB13 cells following treatment with AST-CM

To determine the effects of astrocytes and pericytes on the mRNA expression of rABCG2, TR-BBB13 cells were cultured with AST-CM or PCT-CM (Fig. 6d). After treatment with one-, two- and five-fold concentrated AST-CM, the rABCG2 mRNA levels were 2.92-, 6.26- and 6.50-fold greater than those in non-treated cells, respectively. The mRNA level of mdr1a, which encodes P-gp and is another ABC transporter at the BBB, was 4.82-fold greater than that in non-treated cells following treatment with five-fold concentrated AST-CM. In contrast, treatment with PCT-CM had no significant effect on the level of either mRNA.

Discussion

The present study provides the first evidence that rABCG2 is mainly localized on the luminal side of rat brain capillaries as a functional transporter that forms a disulfide-linked glycoprotein, possibly a homodimer. Furthermore, the rABCG2-mediated transport activity and the rABCG2 mRNA level were increased in BCECs by soluble factor(s) secreted from astrocytes.

The ABCG2 mRNA and protein in the brain capillary fraction were enriched compared with that in rat brain (Figs 1 and 4), suggesting that ABCG2 is predominantly expressed in rat BCECs. Immunohistochemical analysis confirmed that rABCG2 protein is mainly localized at the luminal membrane of brain capillaries in the rat cortex, whereas it was not detected in other brain cells, such as astrocytes and neurons (Fig. 5). As for pericytes, which surround brain capillaries, the expression of rABCG2 remains unclear without more detailed analysis using electronmicroscopy. It has been reported that ABCG2 immunoreactivity was detected in venous and capillary endothelial cells in human peripheral tissues, such as stomach, prostate and ovary, following immunohistochemical analysis (Maliepaard *et al.* 2001), although the function of ABCG2 in these endothelial cells remains obscure.

Although the present study revealed that ABCG2 was localized at the rat BBB, it has been reported that the brain penetration of an ABCG2 substrate was not enhanced in ABCG2 knockout mice (van Herwaarden *et al.* 2003). There could be several explanations for this apparent difference: rABCG2 at the BBB may have a distinct substrate specificity or may not be functional due to species or tissue differences in the sequence and/or the dimer formation of ABCG2. The sequence of rABCG2 was therefore determined using cDNA cloned from rat brain capillary fraction. The clone showed high homology with its human and mouse counterparts. One ABC domain and six TM domains were conserved (Fig. 1b). Furthermore, the amino acids, Q141, E446, R482, N557 and H630, which have been reported to be important for substrate recognition, were conserved (Imai *et al.* 2002; Miwa *et al.* 2003). Mitoxantrone and BODIPY-prazosin were extruded from HEK293/rABCG2myc cells (Fig. 3). Tests show that the substrate specificity is similar to that of mouse and human transporters. These findings suggest that the sequence of rABCG2 is functional at the BBB.

Rat brain capillary fraction, small intestine and kidney highly expressed rABCG2 proteins (Fig. 4), and the tissue distribution of rABCG2 protein is consistent with that of rABCG2 mRNA (Fig. 1a). This is the first report to describe the tissue distribution of rABCG2 at the protein level. Among the tissues tested, rABCG2 in brain capillary fraction is present in the most highly glycosylated form. N-Glycosylation did not alter the level or the pattern of drug resistance mediated by P-gp in transfected cells, although it

contributes to the proper routing or stability of P-gp (Schinkel *et al.* 1993). N-Glycosylation of ABCG2 at the BBB may increase the stability of ABCG2 as far as its membrane localization is concerned.

Although it has been reported that exogenous human ABCG2 forms a homodimer bridged by disulfide bonds in cultured cells (Kage *et al.* 2002), it is still unclear whether ABCG2 functions as a dimer *in vivo*. rABCG2 glycoproteins were detected at the deduced dimeric sizes in rat brain capillary fraction, TR-BBB13 cells, small intestine and kidney under non-reducing conditions (Fig. 4b). The functional expression of rABCG2 in HEK293/rABCG2myc cells indicates that no additional counterpart protein is required for the activity of rABCG2 (Fig. 3), presumably working as a homodimer. Both TR-BBB13 cells and HEK293/rABCG2myc cells exhibited mitoxantrone efflux transport via rABCG2 (Figs 3 and 6). Mitoxantrone resistance was attenuated by inhibiting the homodimer formation of human ABCG2 (Kage *et al.* 2002). These findings strongly suggest that rABCG2 is expressed, at least, as a homodimer bridged by disulfide bonds in rat BCECs.

rABCG2 glycoproteins were detected at the monomeric size as well as the dimeric size in rat brain capillary fraction, TR-BBB13 cells, small intestine and kidney under non-reducing conditions (Fig. 4b). The bands at the monomer size are likely to indicate the premature form of rABCG2 proteins before dimerization, or the existence of non-disulfide-linked rABCG2 proteins. The *Drosophila* homologue of ABCG1 has been reported to have two counterparts, allowing for the transport of different substrates (Ewart *et al.* 1994). TR-BBB13 cells express ABCG1 in addition to ABCG2 (unpublished data). Therefore, dimer formation with ABCG1 may alter the substrate specificity of ABCG2 in rat BCECs.

The efflux transport system at the BBB is important for brain homeostasis and external stimuli may regulate the system. Following treatment with AST-CM, the accumulation of mitoxantrone and BODIPY-prazosin was reduced (Fig. 6a,b). The Ko143-sensitive transport activity of both drugs showed a tendency to increase (Fig. 6c). This result suggests that soluble factors secreted from astrocytes induce ABCG2-mediated transport activity at the BBB. AST-CM increased the rABCG2 mRNA level as well as the Ko143-sensitive transport activity in TR-BBB13 cells (Fig. 6d). In contrast, PCT-CM did not affect either the drug transport activity or the rABCG2 mRNA level. This result suggests that astrocytes under physiological conditions play an important role in regulating ABCG2 function at the BBB, whereas the contribution of pericytes is minor. It has been reported that the expression level of ABCG2 in brain vessels was elevated in glioblastoma (Zhang *et al.* 2003). Glioma cell-derived factors may be involved in the enhancement of the ABCG2 expression as well as normal astrocyte-derived factors.

The Ko143-sensitive transport activity of BODIPY-prazosin continuously increased from one- to five-fold concentrated AST-CM, while the rABCG2 mRNA levels were increased by one-fold concentrated AST-CM and were not significantly increased by higher concentrations (Fig. 6c,d). Therefore, it is possible that both transcriptional regulation and post-translational regulation of rABCG2 function are involved in the functional enhancement of rABCG2. It has been reported that the membrane translocation of ABCG2 was enhanced in hematopoietic stem cells by activating Akt, a serine/threonine kinase (Mogi *et al.* 2003). Our recent investigation has revealed that basic fibroblast growth factor (bFGF), which is known to be an Akt activator, was internalized in BCECs via heparin sulfate proteoglycan expressed on the brain side of the BBB (Deguchi *et al.* 2002). Studies of ABCG2 regulators in AST-CM, including an assessment of how bFGF contributes to this phenomenon, and the difference in the regulators between normal astrocytes and glioma cells should increase our understanding of paracrine interactions between astrocytes and BCECs.

The accumulation of mitoxantrone and BODIPY-prazosin in the presence of Ko143 was also reduced by treatment with AST-CM (Fig. 6a,b), suggesting that AST-CM enhanced the mitoxantrone efflux via mechanisms other than rABCG2 in TR-BBB13 cells. AST-CM increased the level of mdr1a mRNA, encoding P-gp, which transports these drugs as well as ABCG2. Therefore, these findings suggest that the trend of an increase in the rABCG2-unrelated efflux can be partly explained by the up-regulation of P-gp.

The present study strongly suggests that rABCG2 is highly expressed as a functional dimer on the luminal side of brain capillaries. Therefore, it is conceivable that rABCG2 limits the brain penetration of its drug substrates by excreting them to the circulating blood. Indeed, the brain concentration of prazosin after intravenous administration was significantly lower than in other tissues (Dynon *et al.* 1983). It has also been reported that the brain distribution of mitoxantrone is low (Stewart *et al.* 1986). Some hydrophilic compounds present in the brain, such as neurotransmitter metabolites and potential toxins, are excreted from the brain to the circulating blood (Asaba *et al.* 2000; Hosoya *et al.* 2000a; Ohtsuki *et al.* 2002; Mori *et al.* 2003). Among these, dehydroepiandrosterone sulfate (DHEAS) and estrone-3-sulfate are substrates of ABCG2 (Suzuki *et al.* 2003). DHEAS was extruded from a conditionally immortalized mouse BCEC cell line in an ATP-dependent manner (Asaba *et al.* 2000). Taking these findings into consideration, the presence of ABCG2 on the luminal side of the BBB would partly explain the brain-to-blood efflux transport of these endogenous compounds.

It has been reported that coadministration of mitoxantrone and GF120918, which is an inhibitor of ABCG2 and P-gp, did not increase the brain penetration of mitoxantrone (Allen and Schinkel 2002). The present study strongly suggests that

rat BBB expresses ABCG2 which can transport mitoxantrone. Moreover, the rABCG2 expression level in brain capillaries appears to be sufficient for its function to be exhibited, because the intensity of the bands in brain capillary fraction (20 μg/lane) was much greater than that in TR-BBB13 cells (80 μg/lane), which express functional rABCG2 (Fig. 4b). Taken together, these results suggest that rABCG2 is active as an efflux transporter, although other transporter(s) can also exhibit such a function for mitoxantrone. Prazosin is also transported by P-gp (Robey *et al.* 2001), and DHEAS is also transported by MRP4, which has been reported to be expressed in brain capillaries (Zhang *et al.* 2000; Zelcer *et al.* 2003). Further study is needed to elucidate the contribution of ABCG2 to the efflux transport of these compounds across the BBB. Identifying drugs and endogenous compounds that are mainly transported by ABCG2 in the brain is a key issue for clarifying the physiological and pharmacological importance of ABCG2.

In conclusion, the present study demonstrates that rat brain capillaries express functional ABCG2 protein and the transport activity is up-regulated by astrocyte-derived soluble factors. The new finding, that functional ABCG2 is expressed at the rat BBB, contributes to our understanding of the physiological role of ABCG2, and suggests that the influence of ABCG2 as a partner of P-gp cannot be neglected in the development of CNS-acting drugs.

Acknowledgements

The authors wish to thank Dr A. Schinkel (Netherlands Cancer Institute, Amsterdam, the Netherlands) for kindly supplying the ABCG2 inhibitor, Ko143. We would also like to thank Ms. N. Funayama for secretarial assistance. This study was supported, in part, by a Grant-in-Aid for Scientific Research, and a 21st Century Center of Excellence (COE) Program from Japan Society for the Promotion of Science. It was also supported in part by the Industrial Technology Research Grant Program from the New Energy and the Industrial Technology Development Organization (NEDO) of Japan.

References

Allen J. D. and Schinkel A. H. (2002) Multidrug resistance and pharmacological protection mediated by the breast cancer resistance protein (BCRP/ABCG2). *Mol. Cancer Ther.* **1**, 427–434.

Allen J. D., van Loevezijn A., Lakhai J. M., van der Valk M., van Tellingen O., Reid G., Schellens J. H., Koomen G. J. and Schinkel A. H. (2002) Potent and specific inhibition of the breast cancer resistance protein multidrug transporter *in vitro* and in mouse intestine by a novel analogue of fumitremorgin C. *Mol. Cancer Ther.* **1**, 417–425.

Asaba H., Hosoya K., Takanaga H., Ohtsuki S., Tamura E., Takizawa T. and Terasaki T. (2000) Blood–brain barrier is involved in the efflux transport of a neuroactive steroid, dehydroepiandrosterone sulfate, via organic anion transporting polypeptide 2. *J. Neurochem.* **75**, 1907–1916.

Asashima T., Iizasa H., Terasaki T., Hosoya K., Tetsuka K., Ueda M., Obinata M. and Nakashima E. (2002) Newly developed rat brain pericyte cell line, TR-PCT1, responds to transforming growth factor-beta1 and beta-glycerophosphate. *Eur. J. Cell Biol.* **81**, 145–152.

Cooray H. C., Blackmore C. G., Maskell L. and Barrand M. A. (2002) Localisation of breast cancer resistance protein in microvessel endothelium of human brain. *Neuroreport* **13**, 2059–2063.

Deguchi Y., Okutsu H., Okura T., Yamada S., Kimura R., Yuge T., Furukawa A., Morimoto K., Tachikawa M., Ohtsuki S. *et al.* (2002) Internalization of basic fibroblast growth factor at the mouse blood–brain barrier involves perlecan, a heparan sulfate proteoglycan. *J. Neurochem.* **83**, 381–389.

Dobrogowska D. H. and Vorbrodt A. W. (1999) Quantitative immunocytochemical study of blood–brain barrier glucose transporter (GLUT-1) in four regions of mouse brain. *J. Histochem. Cytochem.* **47**, 1021–1030.

Doyle L. A., Yang W., Abruzzo L. V., Krogmann T., Gao Y., Rishi A. K. and Ross D. D. (1998) A multidrug resistance transporter from human MCF-7 breast cancer cells. *Proc. Natl Acad. Sci. USA* **95**, 15665–15670.

Dynon M. K., Jarrott B. and Louis W. J. (1983) Tissue distribution and hypotensive effect of prazosin in the conscious rat. *J. Cardiovasc. Pharmacol.* **5**, 235–239.

Eisenblatter T. and Galla H. J. (2002) A new multidrug resistance protein at the blood–brain barrier. *Biochem. Biophys. Res. Commun.* **293**, 1273–1278.

Eisenblatter T., Huwel S. and Galla H. J. (2003) Characterisation of the brain multidrug resistance protein (BMDP/ABCG2/BCRP) expressed at the blood–brain barrier. *Brain Res.* **971**, 221–231.

Ewart G. D., Cannell D., Cox G. B. and Howells A. J. (1994) Mutational analysis of the traffic ATPase (ABC) transporters involved in uptake of eye pigment precursors in *Drosophila melanogaster*: implications for structure-function relationships. *J. Biol. Chem.* **269**, 10370–10377.

van Herwaarden A. E., Jonker J. W., Wagenaar E., Brinkhuis R. F., Schellens J. H., Beijnen J. H. and Schinkel A. H. (2003) The breast cancer resistance protein (Bcrp1/Abcg2) restricts exposure to the dietary carcinogen 2-amino-1-methyl-6-phenylimidazo[4,5-*b*]pyridine. *Cancer Res.* **63**, 6447–6452.

Hori S., Ohtsuki S., Hosoya K., Nakashima E. and Terasaki T. (2004) A pericyte-derived angiopoietin-1 multimeric complex induces occludin gene expression in brain capillary endothelial cells through Tie-2 activation *in vitro*. *J. Neurochem.* **89**, 503–513.

Hosoya K., Asaba H. and Terasaki T. (2000a) Brain-to-blood efflux transport of estrone-3-sulfate at the blood–brain barrier in rats. *Life Sci.* **67**, 2699–2711.

Hosoya K., Takashima T., Tetsuka K., Nagura T., Ohtsuki S., Takanaga H., Ueda M., Yanai N., Obinata M. and Terasaki T. (2000b) mRNA expression and transport characterization of conditionally immortalized rat brain capillary endothelial cell lines; a new *in vitro* BBB model for drug targeting. *J. Drug Target.* **8**, 357–370.

Hosoya K., Tomi M., Ohtsuki S., Takanaga H., Saeki S., Kanai Y., Endou H., Naito M., Tsuruo T. and Terasaki T. (2002) Enhancement of L-cystine transport activity and its relation to xCT gene induction at the blood–brain barrier by diethyl maleate treatment. *J. Pharmacol. Exp. Ther.* **302**, 225–231.

Imai Y., Nakane M., Kage K., Tsukahara S., Ishikawa E., Tsuruo T., Miki Y. and Sugimoto Y. (2002) C421A polymorphism in the human breast cancer resistance protein gene is associated with low expression of Q141K protein and low-level drug resistance. *Mol. Cancer Ther.* **1**, 611–616.

Jonker J. W., Buitelaar M., Wagenaar E. *et al.* (2002) The breast cancer resistance protein protects against a major chlorophyll-derived

dietary phototoxin and protoporphyria. *Proc. Natl Acad. Sci. USA* **99**, 15649–15654.

Kage K., Tsukahara S., Sugiyama T., Asada S., Ishikawa E., Tsuruo T. and Sugimoto Y. (2002) Dominant-negative inhibition of breast cancer resistance protein as drug efflux pump through the inhibition of S-S dependent homodimerization. *Int. J. Cancer* **97**, 626–630.

Kang Y. S., Ohtsuki S., Takanaga H., Tomi M., Hosoya K. and Terasaki T. (2002) Regulation of taurine transport at the blood–brain barrier by tumor necrosis factor-alpha, taurine and hypertonicity. *J. Neurochem.* **83**, 1188–1195.

Maliepaard M., Scheffer G. L., Faneyte I. F., van Gastelen M. A., Pijnenborg A. C., Schinkel A. H., van De Vijver M. J., Scheper R. J. and Schellens J. H. (2001) Subcellular localization and distribution of the breast cancer resistance protein transporter in normal human tissues. *Cancer Res.* **61**, 3458–3464.

Miwa M., Tsukahara S., Ishikawa E., Asada S., Imai Y. and Sugimoto Y. (2003) Single amino acid substitutions in the transmembrane domains of breast cancer resistance protein (BCRP) alter cross resistance patterns in transfectants. *Int. J. Cancer* **107**, 757–763.

Mogi M., Yang J., Lambert J. F., Colvin G. A., Shiojima I., Skurk C., Summer R., Fine A., Quesenberry P. J. and Walsh K. (2003) Akt signaling regulates side population cell phenotype via Bcrp1 translocation. *J. Biol. Chem.* **278**, 39068–39075.

Mori S., Takanaga H., Ohtsuki S., Deguchi T., Kang Y. S., Hosoya K. and Terasaki T. (2003) Rat organic anion transporter 3 (rOAT3) is responsible for brain-to-blood efflux of homovanillic acid at the abluminal membrane of brain capillary endothelial cells. *J. Cereb. Blood Flow Metab.* **23**, 432–440.

Ohtsuki S., Asaba H., Takanaga H., Deguchi T., Hosoya K., Otagiri M. and Terasaki T. (2002) Role of blood–brain barrier organic anion transporter 3 (OAT3) in the efflux of indoxyl sulfate, a uremic toxin: its involvement in neurotransmitter metabolite clearance from the brain. *J. Neurochem.* **83**, 57–66.

Robey R. W., Honjo Y., van de Laar A., Miyake K., Regis J. T., Litman T. and Bates S. E. (2001) A functional assay for detection of the mitoxantrone resistance protein, MXR (ABCG2). *Biochim. Biophys. Acta* **1512**, 171–182.

Schinkel A. H., Kemp S., Dolle M., Rudenko G. and Wagenaar E. (1993) N-Glycosylation and deletion mutants of the human MDR1 P-glycoprotein. *J. Biol. Chem.* **268**, 7474–7481.

Stewart D. J., Green R. M., Mikhael N. Z., Montpetit V., Thibault M. and Maroun J. A. (1986) Human autopsy tissue concentrations of mitoxantrone. *Cancer Treat. Report* **70**, 1255–1261.

Suzuki M., Suzuki H., Sugimoto Y. and Sugiyama Y. (2003) ABCG2 transports sulfated conjugates of steroids and xenobiotics. *J. Biol. Chem.* **278**, 22644–22649.

Terasaki T., Ohtsuki S., Hori S., Takanaga H., Nakashima E. and Hosoya K. (2003) New approaches to *in vitro* models of blood–brain barrier drug transport. *Drug Discov. Today* **8**, 944–954.

Tetsuka K., Hosoya K., Ohtsuki S., Takanaga H., Yanai N., Ueda M., Obinata M. and Terasaki T. (2001) Acidic amino acid transport characteristics of a newly developed conditionally immortalized rat type 2 astrocyte cell line (TR-AST). *Cell Struct. Funct.* **26**, 197–203.

Zelcer N., Reid G., Wielinga P., Kuil A., van der Heijden I., Schuetz J. D. and Borst P. (2003) Steroid and bile acid conjugates are substrates of human multidrug-resistance protein (MRP) 4 (ATP-binding cassette C4). *Biochem. J.* **371**, 361–367.

Zhang Y., Han H., Elmquist W. F. and Miller D. W. (2000) Expression of various multidrug resistance-associated protein (MRP) homologues in brain microvessel endothelial cells. *Brain Res.* **876**, 148–153.

Zhang W., Mojsilovic-Petrovic J., Andrade M. F., Zhang H., Ball M. and Stanimirovic D. B. (2003) The expression and functional characterization of ABCG2 in brain endothelial cells and vessels. *FASEB J.* **17**, 2085–2087.

JOURNAL OF CELLULAR PHYSIOLOGY 203:378–386 (2005)

PKC/MAPK Signaling Suppression by Retinal Pericyte Conditioned Medium Prevents Retinal Endothelial Cell Proliferation

TETSU KONDO,[1] KEN-ICHI HOSOYA,[3,4] SATOKO HORI,[1,2,4] MASATOSHI TOMI,[3,4] SUMIO OHTSUKI,[1,2,4] AND TETSUYA TERASAKI[1,2,4]*

[1]*Department of Molecular Biopharmacy and Genetics, Graduate School of Pharmaceutical Sciences, Tohoku University, Sendai, Japan*
[2]*New Industry Creation Hatchery Center, Tohoku University, Sendai, Japan*
[3]*Faculty of Pharmaceutical Sciences, Toyama Medical and Pharmaceutical University, Toyama, Japan*
[4]*CREST and SORST of the Japan Science and Technology Agency (JST), Japan*

Little is known about the regulation mechanism of endothelial cell proliferation by retinal pericytes. The purpose of this study was to elucidate the suppression mechanism of retinal capillary endothelial cell growth by soluble factors derived from retinal pericytes. Conditioned medium of retinal pericytes (rPCT1-CM) suppressed ischemia-induced retinal neovascularization. The growth and DNA synthesis of TR-iBRB2 cells, a conditionally immortalized rat retinal capillary endothelial cell line, were suppressed in a concentration-dependent manner by concentrated rPCT1-CM. The number of human cultured endothelial cells was also reduced by rPCT1-CM. These results provide the first evidence that CM from the cultivation of pericytes alone can inhibit retinal neovascularization in vivo and in vitro. Although the growth reduction of TR-iBRB2 cells was only partly reversed by treatment of rPCT1-CM with antibodies to transforming growth factor-β1, it was completely lost by heat-treatment of rPCT1-CM, suggesting that anti-angiogenic factors are soluble proteins. The levels of expression of G1/S-phase-related proteins, such as cyclin D1, cyclin-dependent kinase (cdk)4, cdk6, and proliferating cell nuclear antigen, were reduced and a cdk inhibitor, $p21^{Cip1}$, was induced in rPCT1-CM-treated TR-iBRB2 cells. Moreover, phosphorylated p44/42 mitogen-activated protein kinase (p44/42 MAPK) in TR-iBRB2 cells was reduced by rPCT1-CM treatment and phosphorylated protein kinase C (PKC)α/βII, which is upstream of p44/42 MAPK, was also suppressed. In conclusion, CM from retinal pericytes suppresses PKC-p44/42 MAPK signaling, inhibits endothelial cell growth, and prevents retinal neovascularization. Anti-angiogenic factors derived from retinal pericytes are likely to play a critical role in the regulation of retinal endothelial cell growth. J. Cell. Physiol. 203: 378–386, 2005. © 2004 Wiley-Liss, Inc.

Visual disorders, such as blindness caused by diabetic retinopathy and age-related macular degeneration in adults, and retinopathy of prematurity (ROP) in childhood, lead to a deterioration in the quality of life (Miller et al., 1997; Steinkuller et al., 1999). The common pathological finding of these diseases is proliferation of endothelial cells, namely retinal neovascularization (Campochiaro, 2000). It is very important to elucidate the mechanism of retinal neovascularization, because knowledge of the processes involved may allow the development of new therapies to block retinal angiogenesis.

The pericytes surrounding retinal microvessels are selectively lost in the earliest phase of diabetic retinopathy (Cogan and Kuwabara, 1963). The loss of pericytes induces proliferation of pre-existing retinal capillary endothelial cells and causes formation of abnormal new vessels, in which blood-retinal barrier function is impaired (Hirschi and D'Amore, 1996). Therefore, it appears that retinal pericytes inhibit the irregular growth of endothelial cells. In the processes of retinal neovascularization, endothelial cell growth is mainly stimulated by protein kinase C (PKC)-dependent p44/42 mitogen-activated protein kinase/extracellular signal-regulated kinase (MAPK/ERK) phosphorylation (Shiba et al., 1993; Poulaki et al., 2002). The signaling is activated by vascular endothelial growth factor (VEGF) (Takahashi et al., 1999b). Pigment epithelium-derived factor (PEDF) suppresses ischemia-induced retinal neovascularization due to induction of apoptosis in retinal endothelial cells (Dawson et al., 1999; Stellmach et al., 2001). VEGF and PEDF are expressed in retinal pericytes (Yamagishi et al., 2002). Therefore, this suggests that soluble factors secreted from retinal pericytes play an important role in the regulation of retinal neovascularization. However, it has been reported that conditioned medium (CM) from cultivation of pericytes (or smooth muscle cells) alone failed to inhibit endothelial cell growth (Antonelli-Orlidge et al., 1989; Sato and Rifkin, 1989). This appears to be in conflict with the existence of anti-angiogenic factors, such as PEDF, in retinal pericytes (Martin et al., 2000). Therefore, little is yet known about the mechanism of suppression of endothelial cell proliferation by retinal pericytes.

Although physiological role of retinal pericytes remains largely unknown at present, more information

Contract grant sponsor: Japan Society for the Promotion of Science (Grant-in-Aid for Scientific Research and a 21st Century Center of Excellence (COE) Program); Contract grant sponsor: Industrial Technology Research Grant Program of the New Energy and the Industrial Technology Development Organization (NEDO) of Japan; Contract grant sponsor: Research on Sensory and Communicative Disorders by the Ministry of Health, Labor, and Welfare, Japan.

*Correspondence to: Tetsuya Terasaki, Department of Molecular Biopharmacy and Genetics, Graduate School of Pharmaceutical Sciences, Tohoku University, Aoba, Aramaki, Aoba-ku, Sendai 980-8578, Japan. E-mail: terasaki@mail.pharm.tohoku.ac.jp

Received 20 July 2004; Accepted 2 September 2004

DOI: 10.1002/jcp.20237

for physiological role of brain pericytes is contributed by the use of primary cultured pericytes (Ramsauer et al., 2002) and a conditionally immortalized rat pericyte cell line (Asashima et al., 2002, 2003). Co-culture systems between brain endothelial cells and pericytes afford to elucidate a paracrine interaction between both cells at the blood-brain barrier (Ramsauer et al., 2002; Hori et al., 2004). We have recently established a conditionally immortalized rat retinal endothelial cell line (TR-iBRB2) (Hosoya et al., 2001), and conditionally immortalized rat retinal pericyte cell line (TR-rPCT1) (Kondo et al., 2003) from transgenic rats harboring the temperature-sensitive SV40 large T-antigen gene (tsA58 Tg rats) (Takahashi et al., 1999a). The co-culture system using these conditionally immortalized cell lines could be a useful tool for analyzing the paracrine interaction between capillary endothelial cells and pericytes in the retina. In fact, our published report showed that in contact co-culture with TR-rPCT1 cells, the proliferation of TR-iBRB2 cells was significantly inhibited compared with that of a single culture. However, no such inhibition was observed in non-contact co-culture (Kondo et al., 2003). These results suggest that contact co-culture with TR-rPCT1 cells afforded highly concentrated pericyte-soluble factors in the TR-iBRB2 cells microenvironment. Therefore, we hypothesize that concentration of soluble factors from pericytes is important for the suppression of endothelial cell growth. The suppression of retinal neovascularization by soluble factors in vivo provides important information for the treatment of diabetic retinopathy. The elucidation of the growth mechanism of endothelial cells will increase our understanding of the critical information of physiological role for pericytes and proliferative retinopathy.

The purpose of the present study was to determine whether concentrated CM derived from TR-rPCT1 cells (rPCT1-CM) suppresses retinal neovascularization in vivo, and to elucidate the growth signaling mechanism of TR-iBRB2 cells as indicators of growth regulation by rPCT1-CM.

MATERIALS AND METHODS

Animals

Female C57/BL6J mice at 14 days' gestation were purchased from SLC (Hamamatsu, Japan). All procedures conformed to the provisions of the Animal Care Committee, Graduate School of Pharmaceutical Sciences, Tohoku University and the ARVO Statement on the use of animals in ophthalmic and vision research.

Ischemia-induced retinopathy and subcutaneous injection of rPCT1-CM

A previously described murine model of ischemic-induced retinopathy was set up using dams and neonatal C57/BL6J mice (Smith et al., 1994). Mice in the normal group were maintained under normal room ventilation conditions throughout the experiment. Mice in the ischemic group were exposed with their nursing dams to 75% oxygen from postnatal day 7 (P7) to P12, then removed to room air and injected subcutaneously each day from P12 through P16 with 30 μl Ca^{2+}- and Mg^{2+}-free phosphate-buffered saline [PBS(−)] or 30 μl concentrated rPCT1-CM-dialyzed PBS(−). At P17, all pups were anesthetized and perfused with 1 ml fixative (4% paraformaldehyde/0.1M sodium phosphate buffer, pH 7.4) containing 50 mg 2,000 kDa fluorescein isothiocyanate-labeled dextran (FITC-dextran, Sigma, St. Louis, MO) via the left ventricle of the heart. Eyes were enucleated and placed in fixative. The flat-mounted retinas were viewed under a fluorescence microscope (AxioCam, Zeiss, Thornwood, NY). The ratio of the fluorescence area to total retina area in retinas of mice with ROP was quantified using NIH Image software.

Cell culture

TR-iBRB2, TR-rPCT1, TR-BBB13, and TR-CSFB3 cells were established and characterized as described previously (Hosoya et al., 2000; Hosoya et al., 2001; Kitazawa et al., 2001; Kondo et al., 2003). These rat cell lines were seeded onto rat tail collagen type I-coated tissue culture dishes (BD Biosciences, Bedford, MA). TR-rPCT1 and TR-CSFB3 cells were cultured in Dulbecco's modified Eagle's medium (DMEM; Nissui Pharmaceuticals, Tokyo, Japan) supplemented with 10% fetal bovine serum (FBS; Moregate, Bulimbra, Australia) at 33°C. TR-iBRB2 and TR-BBB13 cells were cultured in DMEM supplemented with 10% FBS and 15 mg/L endothelial cell growth factor (Roche Diagnostics, Mannheim, Germany) at 33°C. The permissive temperature for rat cell lines to be cultured was 33°C, due to the presence of temperature-sensitive SV40 large T-antigen. Human retinal endothelial cells (HREC), human brain microvascular endothelial cells (HBMEC), human umbilical vein endothelial cells (HUVEC), human dermal fibroblasts (HDF), and human skeletal muscle cells (HSkMC) were obtained from Cell Applications (San Diego, CA) or Dainippon Pharmaceutical (Osaka, Japan). These human cells were cultured on rat tail collagen type I-coated tissue culture dishes in basal medium containing growth supplement (Cell Applications) at 37°C. All cells were cultured in a humidified atmosphere of 95% air and 5% CO_2.

Preparation of rPCT1-CM

TR-rPCT1 cells were cultured in 10% FBS DMEM for 48 h. The number of TR-rPCT1 cells was measured, and then 4 ml serum-free DMEM per 1.0×10^6 cells was added to the culture dishes. After 24 h, CM from TR-rPCT1 culture medium was collected and filtered through a 0.22 μm filter. The CM was concentrated up to 20-fold (20×, 10 μg protein/30 μl) using a Centriprep-3 (3 kDa cut-off) (Millipore, Bedford, MA), and then stored at −20°C until required. Normal medium was prepared by the same procedure using serum-free DMEM for control experiments. rPCT1-CM was adjusted to an appropriate concentration by diluting 20× rPCT1-CM with serum-free DMEM for the in vitro study. In the in vivo study, 20× rPCT1-CM was dialyzed against PBS(−) and then concentrated up to 100× (50 μg protein/30 μl) using a Microcon YM-3 (3 kDa cut-off) (Millipore).

Heat treatment and neutralization of transforming growth factor (TGF)-β1 in rPCT1-CM

Heat treatment was carried out by boiling 20× rPCT1-CM for 10 min. The neutralization of TGF-β1 in 20× rPCT1-CM was performed by the addition of 50 μg/ml anti-TGF-β1 neutralizing antibody (R&D systems, Minneapolis, MN) followed by incubation at 4°C for 16 h (Chodon et al., 2000). For experiments, the CM was adjusted to 5× rPCT1-CM containing 10% FBS.

Assay of DNA synthesis activity

TR-iBRB2 cells (1.5×10^3 cells/well) were plated on rat tail collagen type I-coated 96-well plates (BD Biosciences) in 10% FBS DMEM. After 24 h, the culture medium was replaced with rPCT1-CM containing 10% FBS, and the plates were further incubated for 48 h. Then the cells were incubated with 5-bromo-2′-deoxyuridine (BrdU) reagent for 2 h. The BrdU incorporation study was performed by means of Cell Proliferation ELISA (colorimetric) (Roche Diagnostics) according to the manufacturer's protocol.

Western blot analysis of cell cycle-related proteins

TR-iBRB2 cells were cultured in 10% FBS DMEM or 5× rPCT1-CM containing 10% FBS for 48 h. Whole cell lysates were obtained by dissolving cells in lysis buffer containing 10 mM Tris-HCl (pH 7.5), 1% Triton X-100, 0.5% Nonidet P-40, 1 mM EDTA, 150 mM NaCl, 5 mM sodium pyrophosphate, 10 mM *p*-nitrophenyl phosphate, 10 mM β-glycerophosphate, 50 mM sodium fluoride, and 1 mM sodium orthovanadate on ice for 30 min, followed by centrifugation for 10 min at 4°C

and 15,000*g*. Supernatants were separated and used as whole cell extracts. The protein (50 μg) was electrophoresed on an SDS–polyacrylamide gel and electrotransferred to polyvinylidene fluoride membranes. The membranes were incubated with primary antibodies at 4°C for 16 h using blocking agent solution (Block Ace; Dainippon Pharmaceutical). The membranes were washed with 0.1% Tween 20/PBS(−) and incubated with horseradish peroxidase-conjugated secondary antibodies. The bands were visualized with an enhanced chemiluminescence kit (SuperSignal; Pierce, Rockford, IL). Primary antibodies such as cdk2 (1:500), cdk4 (1:250), cyclin D1 (1:250), and $p21^{Cip1}$ (1:500) were from BD Biosciences. Antibodies to cyclin E (1:500) and proliferating cell nuclear antigen (PCNA) (1:1,000) were from Santa Cruz Biotechnology (Santa Cruz, CA). Anti-large T-antigen antibody (1:100) was from Oncogene Research Products (Cambridge, MA) and anti-cdk6 (1:2,500) and anti-β-actin (1:2,000) antibodies were from Sigma.

Phosphorylated status of signal transduction proteins

TR-iBRB2 cells were cultured in 10% FBS DMEM for 24 h. The culture medium was replaced with serum-free DMEM or 5× rPCT1-CM, and then culture was continued for 24 h. Serum-starved TR-iBRB2 cells were treated with serum and then the phosphorylation of signaling proteins was measured by Western blot analysis using the same procedure as in the case of cell cycle-related proteins. Primary antibodies such as total or phosphorylated p44/42 MAPK (1:1,000) and protein kinase B (Akt) (1:1,000), and phosphorylated PKCα/βII (1:1,000) were obtained from Cell Signaling Technology (Beverly, MA). Anti-Ras antibody (1:1,000) was from Upstate Biotechnology (Lake Placid, NY).

Data analysis

Unless otherwise indicated, all data represent the mean ± SEM. An unpaired, two-tailed Student's *t*-test was used to determine the significance of differences between two group means.

RESULTS

Effect of rPCT1-CM on ischemia-induced retinal neovascularization

To assess the anti-angiogenic effect of rPCT1-CM in vivo, ischemia-induced retinopathy mice were perfused with FITC-dextran, and flat-mounted retinas were examined using fluorescence microscopy. Leakage of FITC-dextran was seen in whole mounted retinas when PBS(−) or 20× rPCT1-CM (10 μg protein/30 μl) was subcutaneously administered to pups under ischemic conditions (Fig. 1B or C). In contrast, this leakage was reduced when 100× rPCT1-CM (50 μg protein/30 μl) was subcutaneously administered to pups under ischemic conditions (Fig. 1D). These results show that retinal neovascularization is suppressed in an rPCT1-CM dose-dependent manner. The fluorescence intensity ratio in whole retinas was measured using NIH Image software (Fig. 1E). Although the fluorescence intensity ratio in PBS(−)-treated pups under ischemic conditions was increased 1.89-fold compared with the control, this increase was reduced by 8.05% and 49.4% when 20 and 100× rPCT1-CM were administered to pups under ischemic conditions, respectively. These results support the hypothesis that rPCT1-CM has the ability to suppress ischemia-induced neovascularization in the retina in vivo.

TR-iBRB2 cell growth in rPCT1-CM

The growth of TR-iBRB2 cells was measured in DMEM containing 10% FBS or rPCT1-CM containing 10% FBS (Fig. 2). Following 1× rPCT1-CM treatment, the number of TR-iBRB2 cells was the same as that in 1× normal medium. In contrast, the growth of TR-iBRB2 cells was suppressed in concentrated rPCT1-CM. The number of TR-iBRB2 cells was significantly reduced by 41.0% and 69.1% after 6 days in 2× rPCT1-CM and 5× rPCT1-CM, respectively. The proliferation of TR-iBRB2 cells was suppressed in an rPCT1-CM concentration-dependent manner, suggesting that some cell growth-suppressing factors are secreted from TR-rPCT1 cells. In the following experiments, 5× rPCT1-CM was mainly used to investigate the mechanism of cell growth suppression.

Effect of rPCT1-CM on growth of several types of cultured cells

TR-iBRB2 cells are a conditionally immortalized cell line derived from a tsA58 Tg rat (Hosoya et al., 2001). It is possible that the cell growth suppression in Figure 2 is a typical phenomenon for large T-antigen expressing cells or endothelial cells. Therefore, several types of cells were investigated, and the results are summarized in Table 1. The growth of rat endothelial cell lines TR-iBRB2 and TR-BBB13 and that of human cultured endothelial cells HREC, HBMEC, and HUVEC following 5× rPCT1-CM treatment was suppressed by 65.2%, 62.5%, 61.0%, 50.2%, and 69.8%, respectively. In addition, the cell numbers of a rat epithelial cell line TR-CSFB3, human cultured fibroblasts HDF and skeletal muscle cells HSkMC following 5× rPCT1-CM treatment were reduced by 59.9%, 52.0%, and 24.9%, respectively. However, the number of COS7 cells, transformed by SV40 large T-antigen (Gluzman, 1981), following the 5× rPCT1-CM treatment was not much different from that in normal medium. These results show that soluble factors from TR-rPCT1 cells suppress the growth of several types of cells, that is, an immortalized cell line, endothelial cells from human, epithelial cells, and fibroblasts. Nevertheless, endothelial cells have a greater ability for cell growth suppression by rPCT1-CM than other cell types. This supports the idea that the cell suppression mechanism is not related to the promoter of cell growth in the cell line.

Treatment with TGF-β1-neutralizing antibody or heated rPCT1-CM

TGF-β1 derived from pericytes plays an important role in regulating endothelial cell growth in vitro. Therefore, the number of TR-iBRB2 cells was measured in anti-TGF-β1-antibody-treated rPCT1-CM (Table 2). The growth of TR-iBRB2 cells in 5× rPCT1-CM and in antibody-treated 5× rPCT1-CM was reduced by 71.4% and by 59.4%, respectively. These results suggest that TGF-β1 is one of the anti-angiogenic factors in rPCT1-CM. However, growth only partly recovered in TGF-β1-antibody-treated rPCT-CM. In contrast, the number of TR-iBRB2 cells fully recovered in heated 5× rPCT1-CM culture (Table 2), suggesting that other proteinaceous anti-angiogenic factor(s) exist in rPCT1-CM. Moreover, the TR-iBRB2 cells following rPCT1-CM treatment did not exhibit apoptotic morphology (data not shown), suggesting that the anti-angiogenic effect of rPCT1-CM involved a reduction in cell growth, but not induction of cell death.

rPCT1-CM concentration-dependence of BrdU incorporation

BrdU incorporation by TR-iBRB2 cells was measured at several concentrations of rPCT1-CM (Fig. 3). BrdU incorporation was markedly reduced in an rPCT1-CM

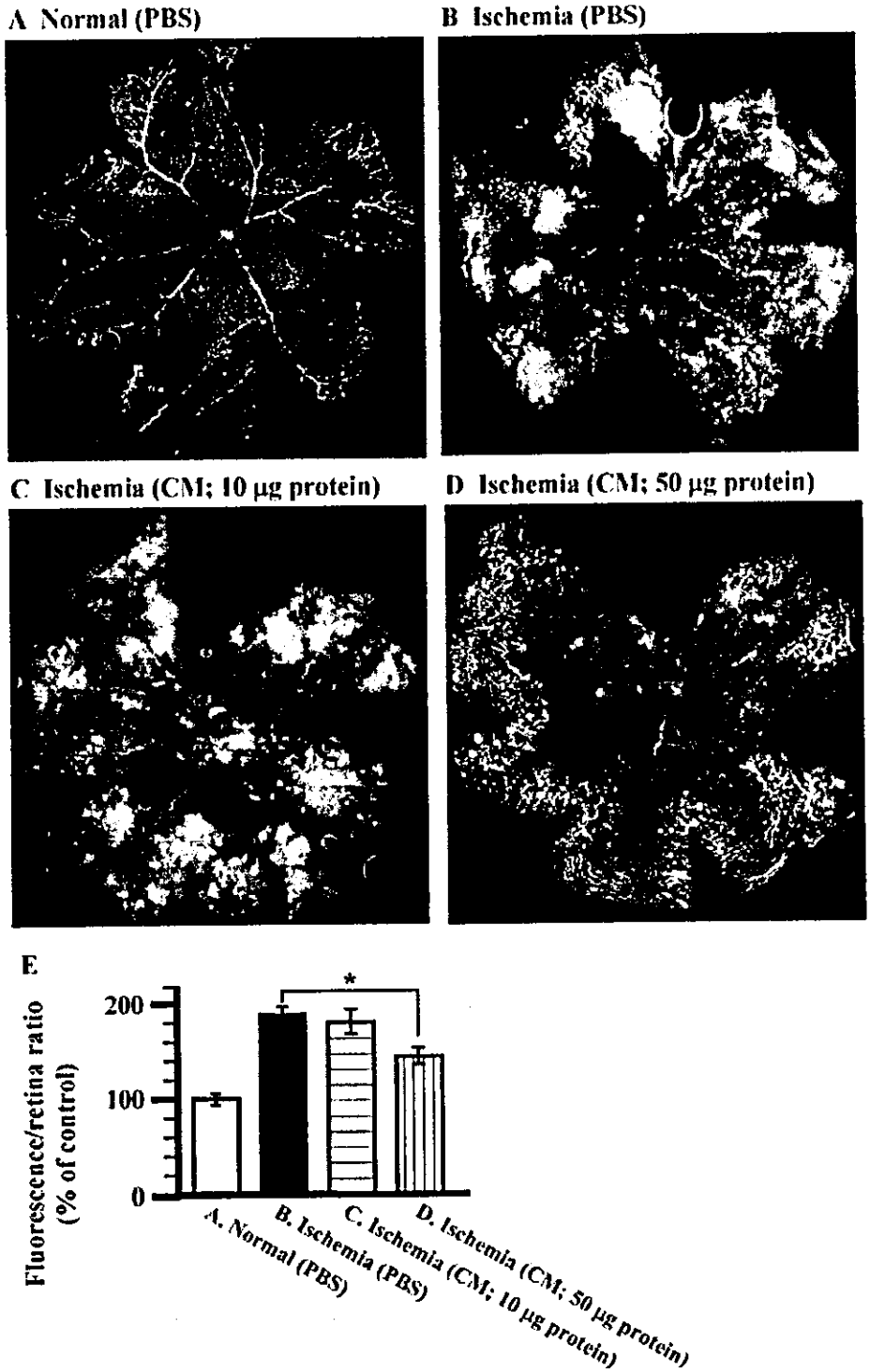

Fig. 1. Effect of rPCT1-CM on retinal neovascularization. A: Mouse pups at P17, kept in a normal room environment, were perfused with 1 ml FITC-dextran solution. B–D: Retinal neovascularization was induced and PBS or rPCT1-CM injected as described under Materials and Methods. B: 30 μl PBS (Ischemia (PBS)), (C) 30 μl 20× rPCT1-CM (10 μg protein)-dialyzed PBS (Ischemia (CM; 10 μg protein)), and (D) 30 μl 100× rPCT1 (50 μg protein)-CM-dialyzed PBS (Ischemia (CM; 50 μg protein)). At P17, the pups were perfused with 1 ml FITC-dextran solution. E: The ratio of the fluorescence area to total retina area in retinas of mice with ROP was quantified. Each column represents the mean ± SEM (n = 6~9). *, $P < 0.05$ significantly different from PBS administration in ischemia.

concentration-dependent manner. BrdU incorporation at 5, 10, and 20× rPCT1-CM was reduced by 22.7%, 42.2%, and 48.8%, respectively. Therefore, rPCT1-CM appears to suppress DNA synthesis and to delay the cell cycle progression in TR-iBRB2 cells.

Expression of cell cycle-related proteins

The G1/S-phase expression of cdks, cyclins, and inhibitors in TR-iBRB2 cells was determined by Western blot analysis (Fig. 4). The 5× rPCT1-CM reduced

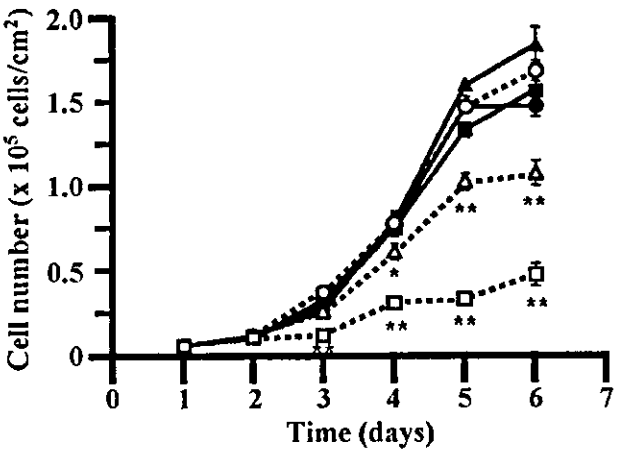

Fig. 2. Comparison of TR-iBRB2 cell growth between normal medium and rPCT1-CM. rPCT1-CM was concentrated using a Centriprep-3 (Millipore). TR-iBRB2 cells were cultured in 1× (closed circles), 2× (closed triangles), and 5× (closed squares) normal medium containing 10% FBS; and 1× (open circles), 2× (open triangles), and 5× (open squares) rPCT1-CM containing 10% FBS. Each point represents the mean ± SEM (n = 3). *, $P < 0.05$ and **, $P < 0.01$, significantly different from the cell number in normal medium.

the expression of cdk4 and cdk6, but not cdk2. The expression of cyclin D1, which forms complexes with cdk4 and cdk6, was reduced by 5× rPCT1-CM. Moreover, cyclin E and PCNA expression was reduced by 5× rPCT1-CM. These results indicate that the expression of G1/S-phase-accelerating proteins in TR-iBRB2 cells is reduced by rPCT1-CM. On the other hand, the expression of $p21^{Cip1}$, a cdk inhibitor, was increased by 5× rPCT1-CM. The expression of large T-antigen was constant in the presence or absence of 5× rPCT1-CM. These results suggest that $p21^{Cip1}$ suppresses the growth of TR-iBRB2 cells in rPCT1-CM, but does not affect SV40 large T-antigen.

Suppression of MAPK and Akt activity by rPCT1-CM

The phosphorylation of p44/42 MAPK and Akt was detected by Western blot analysis when serum-starved TR-iBRB2 cells were cultured with serum. p44/42 MAPK and Akt function as major pathways of cell growth (Dhanasekaran and Reddy, 1998; Vanhaesebroeck and Alessi, 2000). The expression of total and phosphorylated p44/42 MAPK in TR-iBRB2 cells remained at a high level in normal medium and 5× rPCT1-CM up to 120 min after serum stimulation (data not shown). However, phosphorylated p44/42 MAPK was reduced from 3 h after serum stimulation in comparison with TR-iBRB2 cells cultured in normal medium (Fig. 5). Although total Akt protein in TR-iBRB2 cells in 5× rPCT1-CM tended to be reduced in a time-dependent manner, little phosphorylated Akt was detected in normal medium or 5× rPCT1-CM (data not shown). The rPCT1-CM appears to suppress p44/42 MAPK signaling in TR-iBRB2 cells.

TABLE 1. Inhibitory effect of rPCT1-CM on proliferation of several types of cultured cells

Cell types	Percentage of control (%)
Endothelial cells	
TR-iBRB2	34.8 ± 2.4**
TR-BBB13	37.5 ± 1.5**
HREC	39.0 ± 4.0**
HBMEC	49.8 ± 2.5**
HUVEC	30.2 ± 0.4**
Other cells	
TR-CSFB3	40.1 ± 3.8**
HDF	48.0 ± 2.4**
HSkMC	75.1 ± 3.9*
COS7	88.3 ± 13.2

The cells were incubated in 10% FBS DMEM or 5× rPCT1-CM containing 10% FBS for 48 h. Each value represents the mean ± SEM (n = 3).
*, $P < 0.05$ and **, $P < 0.01$ significantly different from control (10% FBS DMEM).

TABLE 2. Effect of TGF-β1-neutralizing antibody and heat treatment of rPCT1-CM on proliferation of TR-iBRB2 cells

Conditions	Percentage of control (%)
DMEM	
Absence of anti-TGF-β1 antibody (control)	100 ± 3
Presence of anti-TGF-β1 antibody	102 ± 7
Heat treatment	86.5 ± 11.6
5× rPCT1-CM	
Absence of anti-TGF-β1 antibody	28.6 ± 3.3*
Presence of anti-TGF-β1 antibody	40.6 ± 1.3*
Heat treatment	127 ± 11

The cells were incubated under each set of conditions for 48 h. Each value represents the mean ± SEM (n = 3).
*, $P < 0.01$ significantly different from control.

Up-stream target of rPCT1-CM for cell growth inhibition

p44/42 MAPK is known to be activated via the PKC or Ras pathway (Yashima et al., 2001). The expression of the phosphorylated form of PKCα/βII or Ras in TR-iBRB2 cells was determined by Western blot analysis. Phosphorylated PKCα/βII in TR-iBRB2 cells was reduced in 5× rPCT1-CM compared with that in normal medium (Fig. 5). On the other hand, Ras was detected in similar amounts in normal medium and 5× rPCT1-CM (Fig. 5). Therefore, inactivation of PKCα/βII-mediated p44/42 MAPK signaling is suggested to cause the suppression of TR-iBRB2 cell growth.

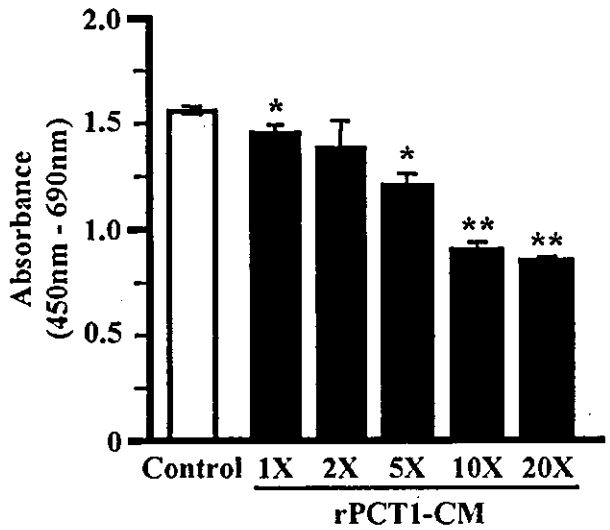

Fig. 3. BrdU incorporation of TR-iBRB2 cells treated with rPCT1-CM. TR-iBRB2 cells were incubated with normal medium (control) or rPCT1-CM for 48 h and then BrdU was incorporated for 2 h. Each column represents the mean ± SEM (n = 3). *, $P < 0.05$ and **, $P < 0.01$ significantly different from the control.

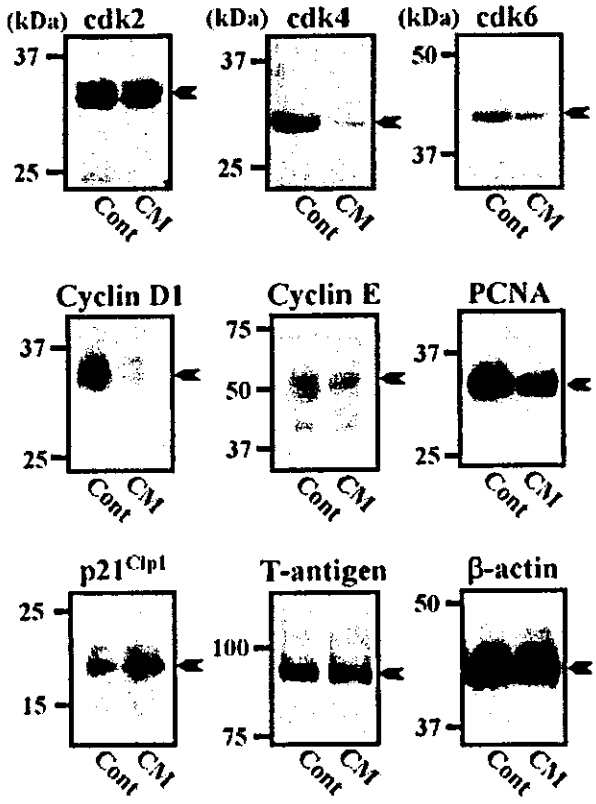

Fig. 4. Western blot analysis of G1 cyclins, cdks, and inhibitors in TR-iBRB2 cells. TR-iBRB2 cells were cultured in DMEM containing 10% FBS until 20% confluence, and then fed DMEM containing 10% FBS (Cont) or 5× rPCT1-CM containing 10% FBS (CM) for 48 h. The arrow on the right-hand side in each picture indicates the expected molecular size. One representative Western blot analysis from at least three independent experiments is shown.

DISCUSSION

The present study demonstrates that soluble factors derived from retinal pericytes suppress ischemia-induced retinal neovascularization. The mechanism of TR-iBRB2 cell growth suppression is the inactivation of the PKCα/βII-mediated p44/42 MAPK signaling pathway and reduction of the expression of cyclin D1, cdk4, and cdk6 (Fig. 6). This is the first report to demonstrate the mechanism of endothelial cell growth suppression by CM derived from retinal pericytes alone.

In the in vivo study, rPCT1-CM administration suppressed retinal neovascularization in a mouse model of ischemia-induced retinopathy (Fig. 1). The diameter of microvessels and leakage of FITC-dextran were reduced following rPCT1-CM administration. In the in vitro study, the number of TR-iBRB2 cells was also reduced following rPCT1-CM (Fig. 2). These suppression effects were observed in an rPCT1-CM concentration-dependent manner. Past reports did not show that CM derived from pericytes alone influenced endothelial cell growth (Antonelli-Orlidge et al., 1989; Sato and Rifkin, 1989). This is probably because of the fact that non-concentrated CM was used. This suggests that concentrated soluble factors from retinal pericytes are important for the suppression of retinal endothelial cell growth. The osmolality of rPCT1-CM (1, 2, and 5×) was not different from the normal medium (1, 2, and 5×) (osmolality: 280 ± 5 mOsm/kg). Therefore, we consider that the suppression of TR-iBRB2 cell growth by rPCT1-CM is due to pericyte-derived anti-angiogenic factors, but not a difference in medium composition. This is the first evidence that soluble factors in rPCT1-CM not only suppress cell growth in vitro, but also play a critical role in controlling retinal neovascularization in vivo.

SV40 large T-antigen, which binds to p53 or retinoblastoma protein (Ray et al., 1996), promotes cell growth. However, cell growth reduction was observed in TR-BBB13 and TR-CSFB3 cells, but not in COS7 cells (Table 1), and the expression of SV40 large T-antigen in TR-iBRB2 cells was the same under normal medium and rPCT1-CM culture conditions (Fig. 4). In addition, the anti-angiogenic effect of rPCT1-CM was also seen with HREC, HBMEC, and HUVEC, but hardly at all with HSkMC (Table 1). This suggests that large T-antigen makes only a minor contribution to the cell growth suppression by rPCT1-CM. Moreover, cell growth suppression by rPCT1-CM appears to exhibit a certain specificity for endothelial cells rather than other cells.

In past reports, latent TGF-β, which is bound to the plasma membrane of pericytes, was activated to TGF-β by plasmin or thrombospondin-1 on the plasma membrane of endothelial cells (Sato and Rifkin, 1989; Crawford et al., 1998). The active TGF-β then inhibited the growth of endothelial cells in vitro. The growth reduction of TR-iBRB2 cells was only partly reversed by treatment of rPCT1-CM with antibodies to TGF-β1, but was completely lost following heat-treatment of rPCT1-CM (Table 2). Although a contribution of TGF-β to cell growth suppression of TR-iBRB2 cells cannot be ruled out, anti-angiogenic soluble proteins (long-chain peptides) are predominantly involved in this suppression. Moreover, rPCT1-CM does not induce cell death as judged from the morphology and unchanged expression of Fas and Fas ligand (FasL) mRNA observed in a cDNA microarray (Atlas Rat Toxicology 1.2 Array, BD Biosciences) in TR-iBRB2 cells (data not shown). Therefore, PEDF, which induces apoptosis via the Fas/FasL pathway (Volpert et al., 2002), may not play a key role in the cell growth-suppressing effect of rPCT1-CM. This suggests that the anti-angiogenic mechanism of rPCT1-CM is related to a reduction in the growth rate of existing endothelial cells in retinal neovascularization (Fig. 1). Moreover, Joussen et al. reported that leukocyte-mediated Fas/FasL-dependent endothelial cell apoptosis led to the breakdown of the blood-retinal barrier in early diabetes (Joussen et al., 2003). If cell growth suppression by rPCT1-CM is not involved in the Fas/FasL pathway, the compound would be a candidate for the treatment of diabetic retinopathy. It remains to be seen, which proteins suppressed cell growth. However, it is also very important to elucidate the growth suppression mechanism involving signal transduction by rPCT1-CM.

The levels of expression of cyclin D1, cdk4, and cdk6 in TR-iBRB2 cells were markedly reduced following rPCT1-CM treatment (Fig. 4). It is known that formation of complexes of cyclin D with cdk4 and cdk6 is particularly important for G1-phase progression of the cell cycle and that the expression of cyclin D1 is induced by growth stimuli via p44/42 MAPK-mediated signaling (Sherr, 1993; Lavoie et al., 1996). Activation of p44/42 MAPK in TR-iBRB2 cells was reduced following rPCT1-CM treatment (Fig. 5), suggesting that the reduction of cyclin D1 expression in TR-iBRB2 cells is also caused by the inactivation of p44/42 MAPK signaling. A recent report indicated that the movement of cyclin D1/cdk4 complex from the cytoplasm to the nuclei induces

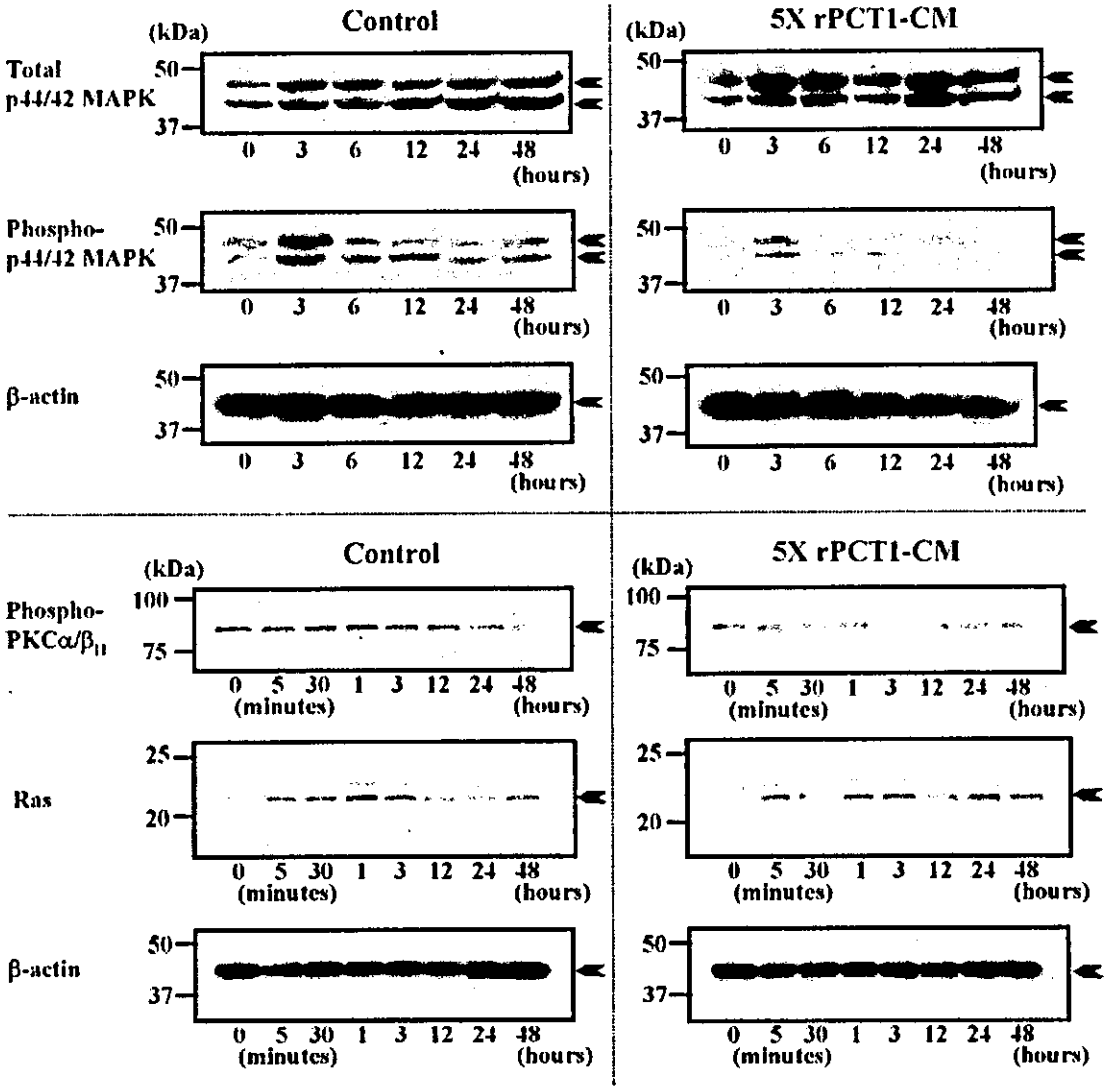

Fig. 5. Time-dependent effects of rPCT1-CM on p44/42 MAPK and PKCα/βII phosphorylation status and Ras expression profile in TR-iBRB2 cells detected by Western blotting analyses. TR-iBRB2 cells were cultured in DMEM containing 10% FBS until 20% confluence and then fed serum-free DMEM or serum-free 5× rPCT1-CM for 24 h. To determine the effect of rPCT1-CM on FBS-stimulated phosphorylation, DMEM containing 10% FBS or 5× rPCT1-CM containing 10% FBS was added to TR-iBRB2 cells after serum-starvation for 24 h. One representative Western blot analysis from at least three independent experiments is shown.

proliferation in rat cardiomyocytes (Tamamori-Adachi et al., 2003). One possibility is that soluble factors in rPCT1-CM not only suppress cell cycle-related proteins, but also reduce the transfer of cyclin D1/cdk4 complex to the nuclei in TR-iBRB2 cells as happens in the case of cardiomyocytes.

The expression of $p21^{Cip1}$ was increased following rPCT1-CM treatment in TR-iBRB2 cells (Fig. 4). It is known that $p21^{Cip1}$ forms a complex with cdk4/6 to inhibit cell growth and is induced by p53 (El-Deiry et al., 1993; Xiong et al., 1993). The p53 in TR-iBRB2 and COS7 cells would be inactivated because of introduction of large T-antigen gene (Gluzman, 1981; Hosoya et al., 2001). However, rPCT1-CM did not suppress COS7 cell growth (Table 1). Therefore, it appears that induction of $p21^{Cip1}$ expression by rPCT1-CM occurs via a p53-independent pathway and prevents cell cycle progression in TR-iBRB2 cells. On the other hand, Rössig et al. reported that Akt-dependent phosphorylation in $p21^{Cip1}$ promotes cell growth because of induction of PCNA and cdk4, which activates DNA polymerase δ and increases the formation of cyclin D/cdk4 complex, respectively (Rössig et al., 2001). The phosphorylated form of Akt was not detected in TR-iBRB2 cells (data not shown). Therefore, it is unlikely that $p21^{Cip1}$ functions as a cell growth accelerator in TR-iBRB2 cells. The expression of PCNA was reduced following rPCT1-CM treatment in TR-iBRB2 cells (Fig. 4). Moreover, the reduction in BrdU incorporation in TR-iBRB2 cells was rPCT1-CM concentration-dependent (Fig. 3). This suggests that the reduction of PCNA activity by rPCT1-CM leads to suppression of DNA synthesis and proliferation. Osuga et al. reported that flavopiridol, a cdk inhibitor, prevents neuronal death by ischemia in rat brain, suggesting that cdks are useful therapeutic targets for neurodegenerative disorders (Osuga et al., 2000). rPCT1-CM down-regulates cdk4/6 and up-regulates $p21^{Cip1}$ (Fig. 4), which suggests that soluble factors from retinal

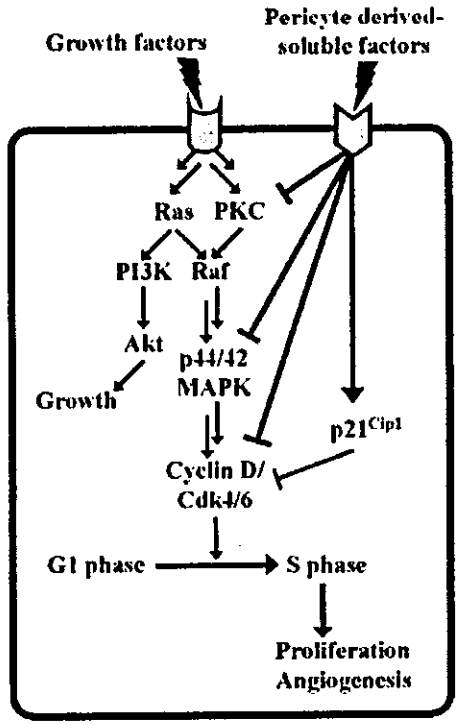

Fig. 6. Putative mechanisms underlying signaling suppression of endothelial cell proliferation involving retinal neovascularization by soluble factors derived from retinal pericytes.

pericytes offer partial neuroprotection for retinal nerve cells.

The reduction of phosphorylated p44/42 MAPK in TR-iBRB2 cells treated with rPCT1-CM was time-dependent, but the activated form of Akt was not detected (Fig. 5), suggesting that p44/42 MAPK-mediated signaling is reduced for a short time following rPCT1-CM and that this leads to suppression of endothelial cell growth. The signal transduction of p44/42 MAPK via PKC or Ras is dependent on the origin of the endothelial cells (Yashima et al., 2001). The phosphorylation of PKCα/βII was suppressed by rPCT1-CM in TR-iBRB2 cells, although the Ras expression was similar to that of control medium (Fig. 5). Persistent hyperglycemia in diabetes stimulates production of diacylglycerol and induces ischemia, resulting in activation of PKCβII-p44/42 MAPK in retinal endothelial cells, which is also detected in mice with ischemia-induced retinopathy (Aiello et al., 1997; Kampik and Gandorfer, 2000; Poulaki et al., 2002; Suzuma et al., 2002). Moreover, retinal neovascularization was inhibited by oral administration of a PKC inhibitor, CGP 41251 (Seo et al., 1999). This suggests that soluble factors derived from retinal pericytes suppress PKCβII-dependent p44/42 MAPK signaling in diabetic retinopathy and that loss of pericytes leads to stimulation of the signaling in retinal endothelial cells.

In conclusion, this study provides the first evidence that soluble factors from retinal pericytes suppress the activation of PKC-p44/42 MAPK signaling and the expression of cyclin D1, cdk4, and cdk6, inhibit endothelial cell growth in vitro, and prevent retinal neovascularization in vivo (Fig. 6). As the number of diabetic patients is increasing throughout the world, acquired blindness is a serious problem. Soluble factors derived from retinal pericytes may help protect diabetic patients from visual disorders.

ACKNOWLEDGMENTS

We thank Dr. Y. Obara and Dr. T. Nakazawa for valuable discussions and Ms. N. Funayama for secretarial assistance.

LITERATURE CITED

Aiello LP, Bursell SE, Clermont A, Duh E, Ishii H, Takagi C, Mori F, Ciulla TA, Ways K, Jirousek M, Smith LE, King GL. 1997. Vascular endothelial growth factor-induced retinal permeability is mediated by protein kinase C in vivo and suppressed by an orally effective β-isoform-selective inhibitor. Diabetes 46:1473–1480.

Antonelli-Orlidge A, Saunders KB, Smith SR, D'Amore PA. 1989. An activated form of transforming growth factor β is produced by cocultures of endothelial cells and pericytes. Proc Natl Acad Sci USA 86:4544–4548.

Asashima T, Iizasa H, Terasaki T, Hosoya K, Tetsuka K, Ueda M, Obinata M, Nakashima E. 2002. Newly developed rat brain pericyte cell line, TR-PCT1, responds to transforming growth factor-β1 and β-glycerophosphate. Eur J Cell Biol 81:145–152.

Asashima T, Iizasa H, Terasaki T, Nakashima E. 2003. Rat brain pericyte cell lines expressing β2-adrenergic receptor, angiotensin II receptor type 1A, klotho, and CXCR4 mRNAs despite having endothelial cell markers. J Cell Physiol 197:69–76.

Campochiaro PA. 2000. Retinal and choroidal neovascularization. J Cell Physiol 184:301–310.

Chodon T, Sugihara T, Igawa HH, Funayama E, Furukawa H. 2000. Keloid-derived fibroblasts are refractory to Fas-mediated apoptosis and neutralization of autocrine transforming growth factor-β1 can abrogate this resistance. Am J Pathol 157:1661–1669.

Cogan DG, Kuwabara T. 1963. Capillary shunts in the pathogenesis of diabetic retinopathy. Diabetes 12:293–300.

Crawford SE, Stellmach V, Murphy-Ullrich JE, Ribeiro SM, Lawler J, Hynes RO, Boivin GP, Bouck N. 1998. Thrombospondin-1 is a major activator of TGF-β1 in vivo. Cell 93:1159–1170.

Dawson DW, Volpert OV, Gillis P, Crawford SE, Xu H, Benedict W, Bouck NP. 1999. Pigment epithelium-derived factor: A potent inhibitor of angiogenesis. Science 285:245–248.

Dhanasekaran N, Reddy EP. 1998. Signaling by dual specificity kinases. Oncogene 17:1447–1455.

El-Deiry WS, Tokino T, Velculescu VE, Levy DB, Parsons R, Trent JM, Lin D, Mercer WE, Kinzler KW, Vogelstein B. 1993. WAF1, a potential mediator of p53 tumor suppression. Cell 75:817–825.

Gluzman Y. 1981. SV40-transformed simian cells support the replication of early SV40 mutants. Cell 23:175–182.

Hirschi KK, D'Amore PA. 1996. Pericytes in the microvasculature. Cardiovasc Res 32:687–698.

Hori S, Ohtsuki S, Hosoya K, Nakashima E, Terasaki T. 2004. A pericyte-derived angiopoietin-1 multimeric complex induces occludin gene expression in brain capillary endothelial cells through Tie-2 activation in vitro. J Neurochem 89:503–513.

Hosoya K, Takashima T, Tetsuka K, Nagura T, Ohtsuki S, Takanaga H, Ueda M, Yanai N, Obinata M, Terasaki T. 2000. mRNA expression and transport characterization of conditionally immortalized rat brain capillary endothelial cell lines; a new in vitro BBB model for drug targeting. J Drug Target 8:357–370.

Hosoya K, Tomi M, Ohtsuki S, Takanaga H, Ueda M, Yanai N, Obinata M, Terasaki T. 2001. Conditionally immortalized retinal capillary endothelial cell lines (TR-iBRB) expressing differentiated endothelial cell functions derived from a transgenic rat. Exp Eye Res 72:163–172.

Joussen AM, Poulaki V, Mitsiades N, Cai WY, Suzuma I, Pak J, Ju ST, Rook SL, Esser P, Mitsiades CS, Kirchhof B, Adamis AP, Aiello LP. 2003. Suppression of Fas-FasL-induced endothelial cell apoptosis prevents diabetic blood-retinal barrier breakdown in a model of streptozotocin-induced diabetes. FASEB J 17:76–78.

Kampik A, Gandorfer A. 2000. Medical treatment of diabetic retinopathy. In: van Bijsterveld OP, editor. Diabetic retinopathy. 1st edition. London: Martin Dunitz. pp 65–78.

Kitazawa T, Hosoya K, Watanabe M, Takashima T, Ohtsuki S, Takanaga H, Ueda M, Yanai N, Obinata M, Terasaki T. 2001. Characterization of the amino acid transport of new immortalized choroid plexus epithelial cell lines: A novel in vitro system for investigating transport functions at the blood-cerebrospinal fluid barrier. Pharm Res 18:16–22.

Kondo T, Hosoya K, Hori S, Tomi M, Ohtsuki S, Takanaga H, Nakashima E, Iizasa H, Asashima T, Ueda M, Obinata M, Terasaki T. 2003. Establishment of conditionally immortalized rat retinal pericyte cell lines (TR-rPCT) and their application in a co-culture system using retinal capillary endothelial cell line (TR-iBRB2). Cell Struct Funct 28:145–153.

Lavoie JN, L'Allemain G, Brunet A, Muller R, Pouyssegur J. 1996. Cyclin D1 expression is regulated positively by the p42/p44MAPK and negatively by the p38/HOGMAPK pathway. J Biol Chem 271:20608–20616.

Martin AR, Bailie JR, Robson T, McKeown SR, Al-Assar O, McFarland A, Hirst DG. 2000. Retinal pericytes control expression of nitric oxide synthase and endothelin-1 in microvascular endothelial cells. Microvasc Res 59:131–139.

Miller JW, Adamis AP, Aiello LP. 1997. Vascular endothelial growth factor in ocular neovascularization and proliferative diabetic retinopathy. Diabetes Metab Rev 13:37–50.

Osuga H, Osuga S, Wang F, Fetni R, Hogan MJ, Slack RS, Hakim AM, Ikeda JE, Park DS. 2000. Cyclin-dependent kinases as a therapeutic target for stroke. Proc Natl Acad Sci USA 97:10254–10259.

Poulaki V, Qin W, Joussen AM, Hurlbut P, Wiegand SJ, Rudge J, Yancopoulos GD, Adamis AP. 2002. Acute intensive insulin therapy exacerbates diabetic

blood-retinal barrier breakdown via hypoxia-inducible factor-1α and VEGF. J Clin Invest 109:805–815.
Ramsauer M, Krause D, Dermietzel R. 2002. Angiogenesis of the blood-brain barrier in vitro and the function of cerebral pericytes. FASEB J 16: 1274–1276.
Ray S, Anderson ME, Tegtmeyer P. 1996. Differential interaction of temperature-sensitive simian virus 40 T antigens with tumor suppressors pRb and p53. J Virol 70:7224–7227.
Rössig L, Jadidi AS, Urbich C, Badorff C, Zeiher AM, Dimmeler S. 2001. Akt-dependent phosphorylation of $p21^{Cip1}$ regulates PCNA binding and proliferation of endothelial cells. Mol Cell Biol 21:5644–5657.
Sato Y, Rifkin DB. 1989. Inhibition of endothelial cell movement by pericytes and smooth muscle cells: Activation of a latent transforming growth factor-beta 1-like molecule by plasmin during co-culture. J Cell Biol 109:309–315.
Seo MS, Kwak N, Ozaki H, Yamada H, Okamoto N, Yamada E, Fabbro D, Hofmann F, Wood JM, Campochiaro PA. 1999. Dramatic inhibition of retinal and choroidal neovascularization by oral administration of a kinase inhibitor. Am J Pathol 154:1743–1753.
Sherr CJ. 1993. Mammalian G1 cyclins. Cell 73:1059–1065.
Shiba T, Inoguchi T, Sportsman JR, Heath WF, Bursell S, King GL. 1993. Correlation of diacylglycerol level and protein kinase C activity in rat retina to retinal circulation. Am J Physiol 265:E783–E793.
Smith LE, Wesolowski E, McLellan A, Kostyk SK, D'Amato R, Sullivan R, D'Amore PA. 1994. Oxygen-induced retinopathy in the mouse. Invest Ophthalmol Vis Sci 35:101–111.
Steinkuller PG, Du L, Gilbert C, Foster A, Collins ML, Coats DK. 1999. Childhood blindness. J AAPOS 3:26–32.
Stellmach V, Crawford SE, Zhou W, Bouck N. 2001. Prevention of ischemia-induced retinopathy by the natural ocular antiangiogenic agent pigment epithelium-derived factor. ProcNatl Acad Sci USA 98:2593–2597.
Suzuma K, Takahara N, Suzuma I, Isshiki K, Ueki K, Leitges M, Aiello LP, King GL. 2002. Characterization of protein kinase C β isoform's action on retinoblastoma protein phosphorylation, vascular endothelial growth factor-induced endothelial cell proliferation, and retinal neovascularization. Proc Natl Acad Sci USA 99:721–726.
Takahashi R, Hirabayashi M, Yanai N, Obinata M, Ueda M. 1999a. Establishment of SV40-tsA58 transgenic rats as a source of conditionally immortalized cell lines. Exp Anim 48:255–261.
Takahashi T, Ueno H, Shibuya M. 1999b. VEGF activates protein kinase C-dependent, but Ras-independent Raf-MEK-MAP kinase pathway for DNA synthesis in primary endothelial cells. Oncogene 18:2221–2230.
Tamamori-Adachi M, Ito H, Sumrejkanchanakij P, Adachi S, Hiroe M, Shimizu M, Kawauchi J, Sunamori M, Marumo F, Kitajima S, Ikeda MA. 2003. Critical role of cyclin D1 nuclear import in cardiomyocyte proliferation. Circ Res 92:e12–e19.
Vanhaesebroeck B, Alessi DR. 2000. The PI3K-PDK1 connection: more than just a road to PKB. Biochem J 346:561–576.
Volpert OV, Zaichuk T, Zhou W, Reiher F, Ferguson TA, Stuart PM, Amin M, Bouck NP. 2002. Inducer-stimulated Fas targets activated endothelium for destruction by anti-angiogenic thrombospondin-1 and pigment epithelium-derived factor. Nat Med 8:349–357.
Xiong Y, Hannon GJ, Zhang H, Casso D, Kobayashi R, Beach D. 1993. p21 is a universal inhibitor of cyclin kinases. Nature 366:701–704.
Yamagishi S, Inagaki Y, Amano S, Okamoto T, Takeuchi M. 2002. Up-regulation of vascular endothelial growth factor and down-regulation of pigment epithelium-derived factor messenger ribonucleic acid levels in leptin-exposed cultured retinal pericytes. Int J Tissue React 24:137–142.
Yashima R, Abe M, Tanaka K, Ueno H, Shitara K, Takenoshita S, Sato Y. 2001. Heterogeneity of the signal transduction pathways for VEGF-induced MAPKs activation in human vascular endothelial cells. J Cell Physiol 188:201–210.